Projector color.
Buerger Award

ACA Boston July 22 50 mins 2012

The future of Diffraction Physics in Crystallography

John C H Spence*

ASU Physics/LBNL

*and many others, especially

Henry Chapman, Uwe Weierstall, J.M. Zuo, Bruce Doak, Anton Barty,
Ilme Schlichting, Petra Fromme……

OUTLINE
TWO REVOLUTIONS: LENSLESS IMAGING; SNAPSHOT FSX

* Buerger's life's work. Is PX unique ?
* CBED, diffractive imaging, powder flipping.
*Experimental method of serial femtosecond nanocrystallography (sFX). Data analysis.
* Milestones in sFX:

Atomic resolution
New biology
Time resolved nanocrystallography
Single particle methods, snapshot chemistry, future plans.

Martin J. Buerger 1903 – 1986 MNAS
An american "Bragg" ?

Professor of Mineralogy at MIT (also JMC, Warren 1953)
Inventor of the Precession camera
Author of 12 textbooks on XRC, 200 papers, Int. Tables – "exhaustive thoroughness"
Solved mineral structures, soap - (without computer !), inspired by Bragg's 1927 talk at MIT.
Extinction, polymorphism, twinning, powder diffraction.
"Buergerite" named for him.
"Vector Spaces" – Image seeking methods for finding heavy atoms from Patterson.
Optical reconstruction following Bragg 1939 – i) Use polarizer for centro phases
ii) Make holes propn to F^2 to get Patterson.
iii) Use positive of X-ray film as mask in bfp. –
get directly a photograph of projected density map for centro xtals ! (use polarizer for phase).

Uniqueness in Crystallography. Can two different xtals have the same diffraction pattern ?

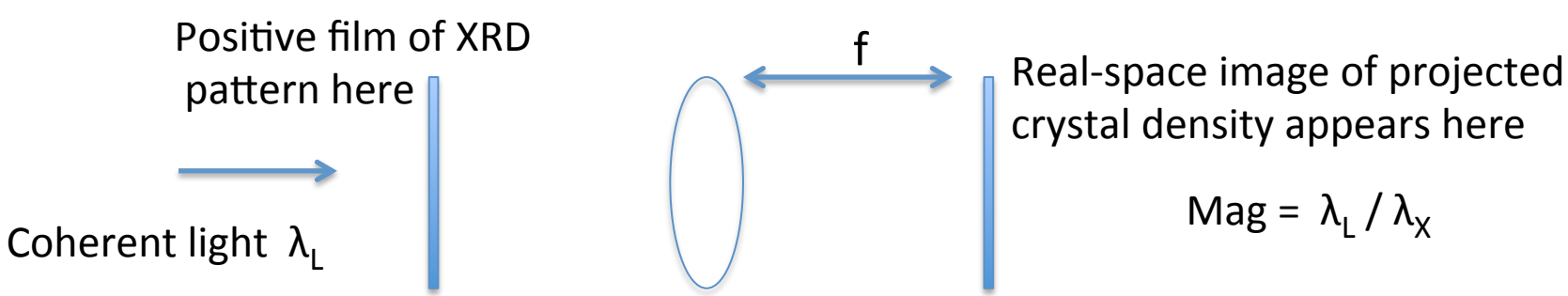

Homometric structures – different xtals with same diffraction patterns.

One family of homometric structures (Hoseman and Bagchi, Acta Cryst 7, p. 237 (1954)) may be generated using the result that…..

$$\rho_1(r) = l(r) * m(r)$$

$$and$$

$$\rho_2(r) = l(r) * m^*(-r)$$

Bixbyite Pauling 1936

$$have \quad same \quad Fourier \quad modulus \quad |R(u)|, \quad since$$

$$R_1(u) = L(u)M(u) \quad and \quad R_2(u) = L(u)M^*(u)$$

If l(r) is a lattice and m(r) a molecule, then m, m* are enants, but ρ_1, ρ_2 are not enants.

Example:

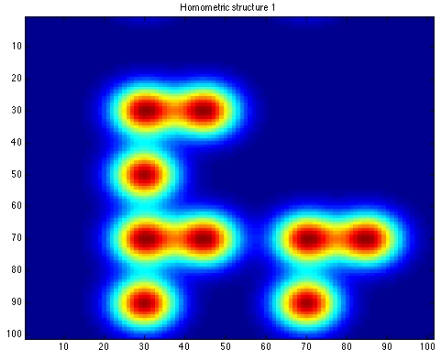

Homo1

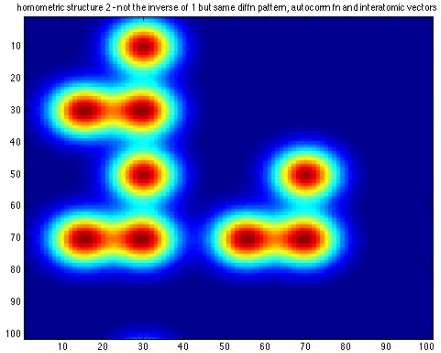

Homo2

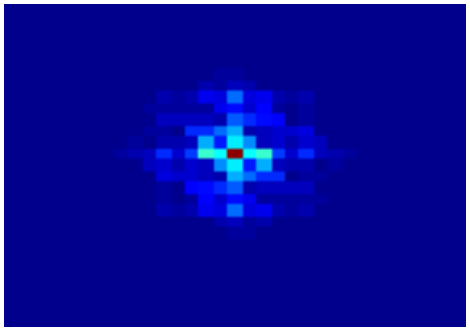

Fourier Mod of either

Note: Homo1 is not the inverse (enantiomorph) of Homo2.

Distinguished by Multiple scattering ELNES

Conclusion: HiO could not distinguish these unless tight support provided.

A different data set, showing "heavy-atom" method.

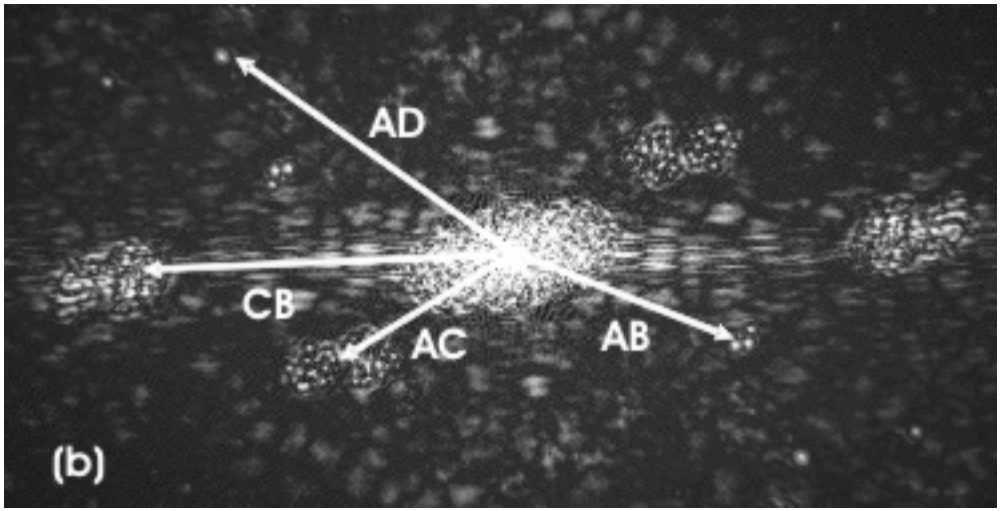

Autocorrelation from X-ray intensity
- a map of all interball vectors.

Friedel symm is a test for a real object.

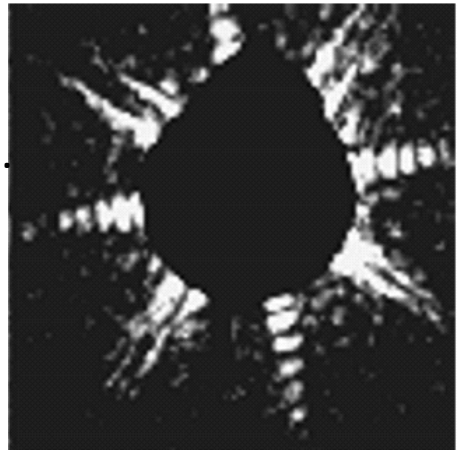

Sinc pattern from SiN window around beam stop.

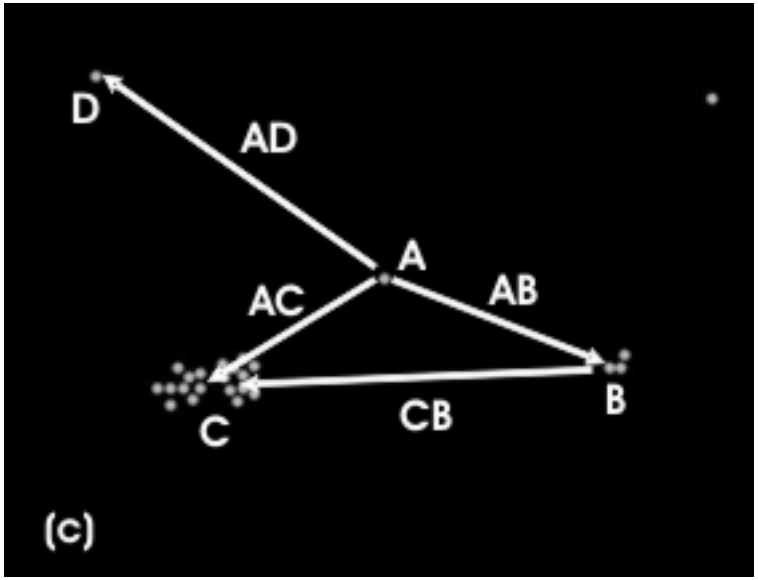

SEM real-space image

Note how balls at B are faithfully imaged in ball A in the autocorrelation function $=\rho(r)*\rho(-r)$ at AB in figure (b)

This suggests using AFM to place single ball near unknown (eg cell). Autocorrelation then gives image and better support.

Support obtained from sem image.

Acta A.59, 143 (2003).

Is it possible to reconstruct without any knowledge of support ?

Get support of object from support of autocorrelation - then "shrink-wrap" to avoid previous subjective estimate of boundary.

Notes:
First estimate of boundary (support) is boundary (4% threshold) of autocorr.

Autocorr is centric, object not.

Boundary of autocorr shrinks as HiO improves estimate. Every 20 itns make new support at 20% threshold.

Inversion symm eventually lost !

Intensity obscured by beamstop "floats" during iterations.

Cf Solvent flattening.

Marchesini,He,Howells,Chapman,Weierstall,Spence. Phys Rev B. 2003 .

Object estimate | Support estimate

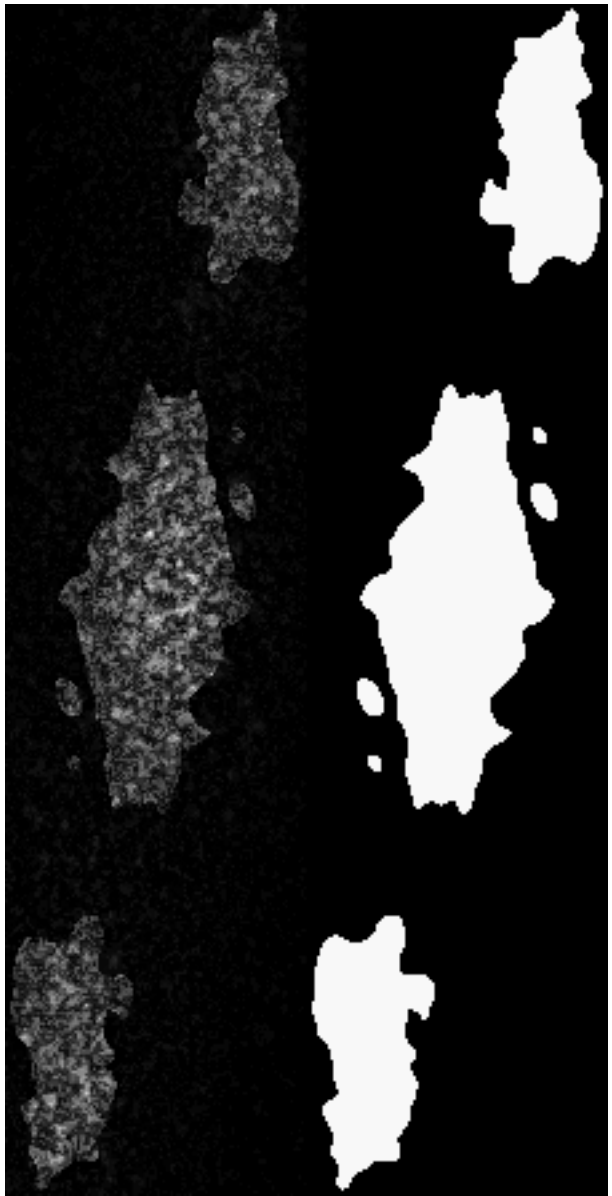

50nm Gold Balls

λ=2.1nm

ALS LBL Expts LBL $

We demonstrated Lensless soft-X-ray tomography at 10nm resolution

Object is 50nm gold balls decorating the sides of a SiN pyramid

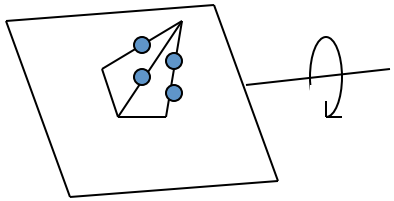

SiN

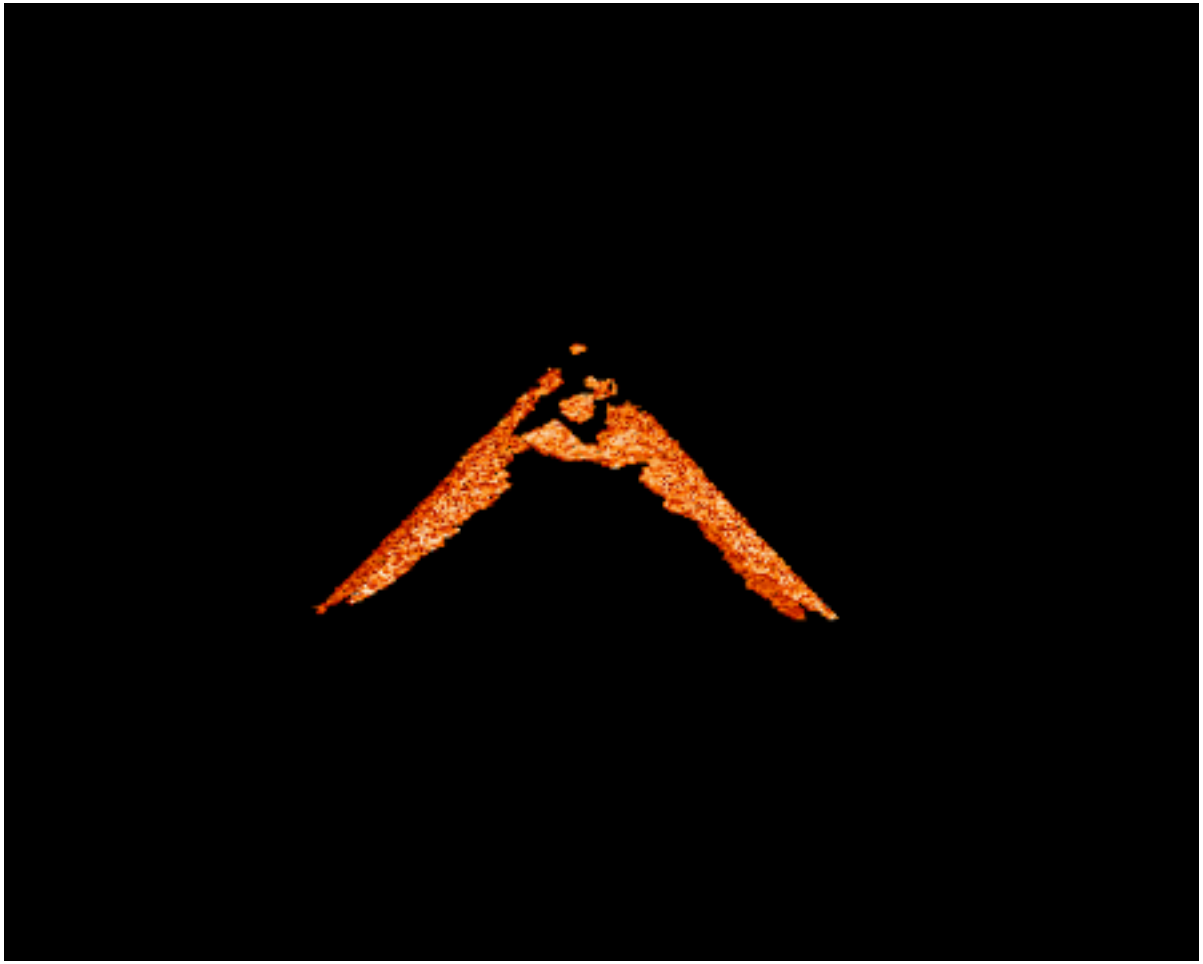

The X-ray beam energy is 650 eV. (Oxygen edge is 580 eV)

Wavelength about 1.8nm

Undulator on synchrotron (ALS, LBL, Berkeley)

3D reconstruction of real-space density from phased 3D diffraction data. Interations consist of several hundred 1024^3=8GB complex FFT. 5 arrays. Takes 20 hrs for 3000 iterations on 16 node Mac G5 cluster at LLNL (Barty)

Chapman, Barty, Marchesini, Cui, Howells, Spence, Weierstall J. Opt Soc Am. 23, p.1179 (2006)

First atomic-resolution image of a DWNT by any method.

Obtained by HiO. Aberration-free.

Gives ID, OD, Chiral vectors.

Zuo et al Sceince 2003.

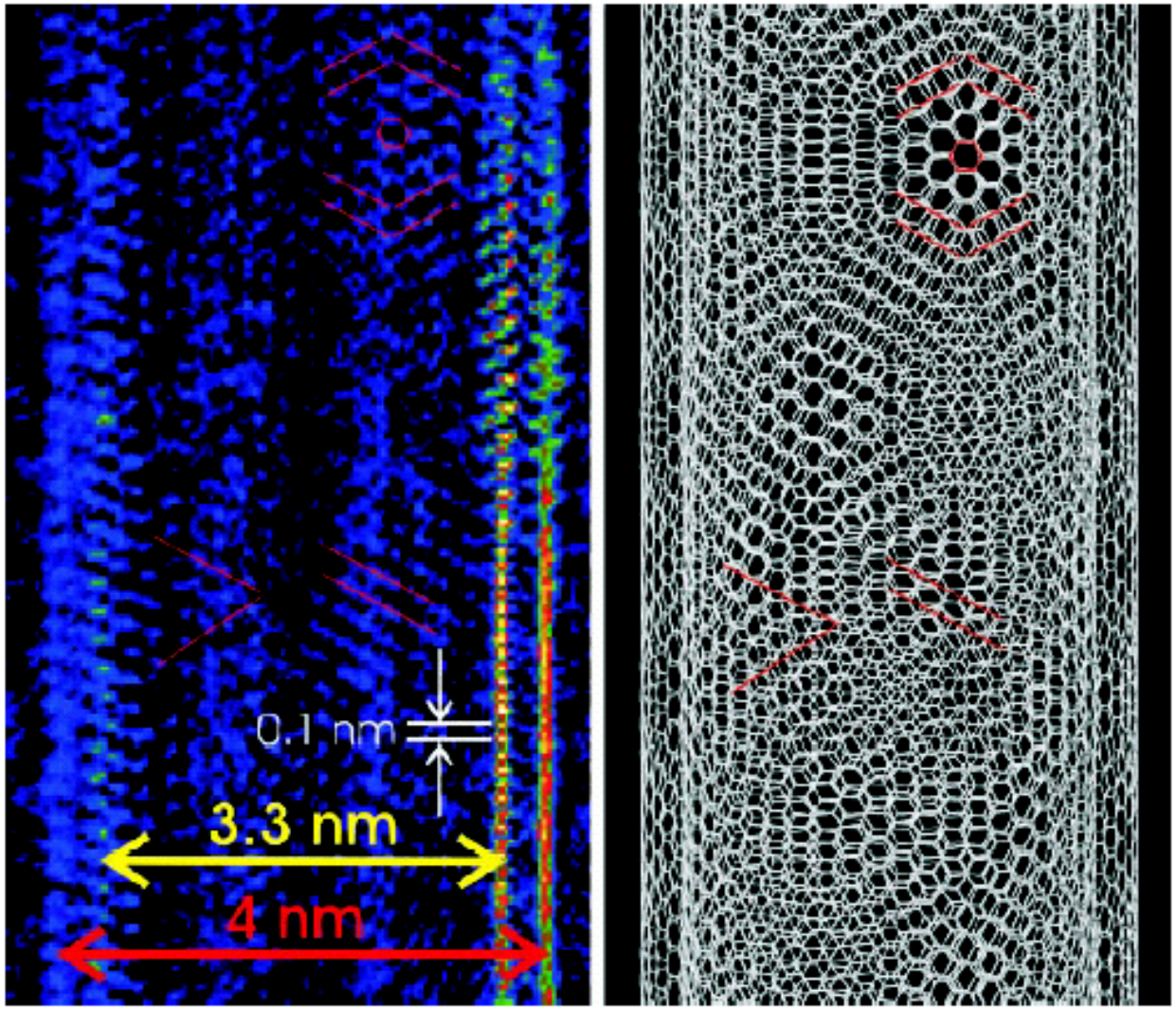

Fig. 2. (**left**) A section of the reconstructed DWNT image at 1-Å resolution and (**right**) a structural model constructed with the use of the chiral vectors of (35, 25) and (26, 24) that were determined from the image and diffraction pattern. The DWNT imaged here is one of many in our catalytic chemical vapor deposition–grown samples. Yellow and red lines mark the diameters of the inner and outer tubes, respectively. One side of walls is stronger than the other, which is because of the illumination. The DWNT is incommensurate. In projection, the structure has complex patterns showing both accidental coincidences and Moiré fringes, which are highlighted by hexagons and lines.

Making electron diffraction in a TEM quantitative.

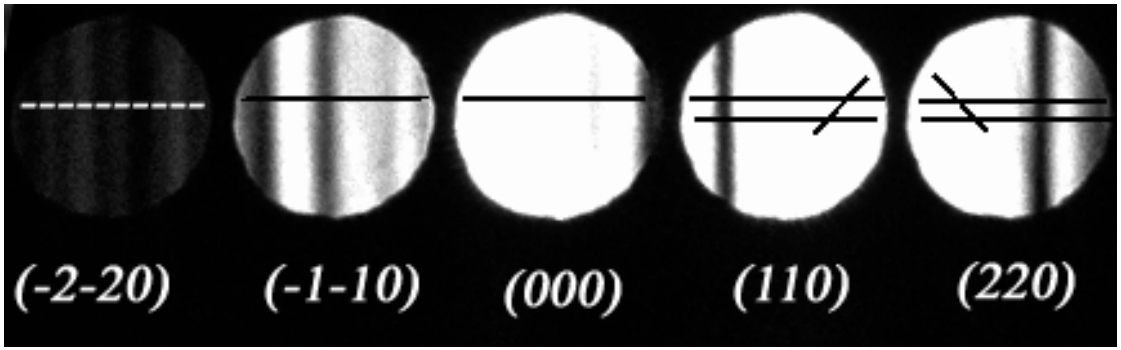

Convergent-beam diffraction from Rutile – elastic energy filtered. Experiment vs theory.

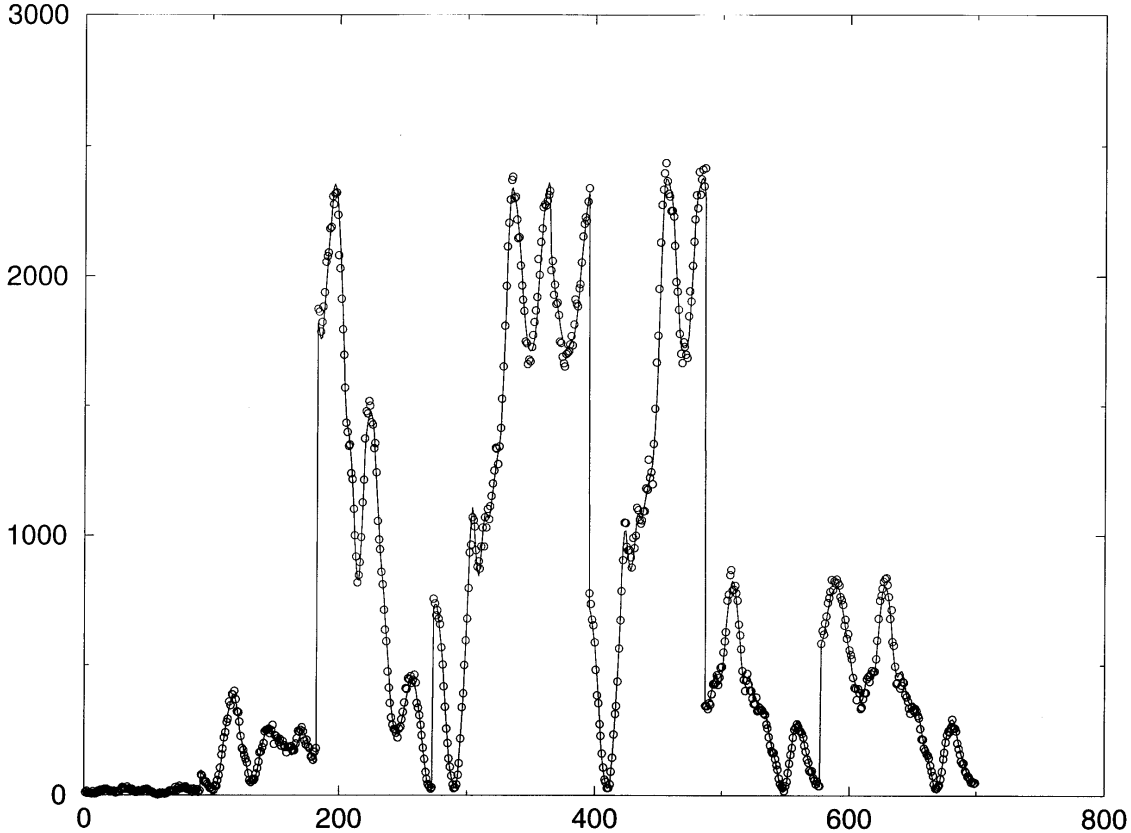

Example of CBED refinement. Top image shows systematic row for (110) and (220) of rutile crystal with line scans used.

Below shows the pixel values (circles) compared with calculated values (solid line). The χ^2 for this fit is 1.2.

CCD characterization (MTF, DQE) important. See Zuo, Micros Res and Techn. 49, p. 245 (2000).

Seeing bonds – charge-density refinement for cuprite by electron diffraction*

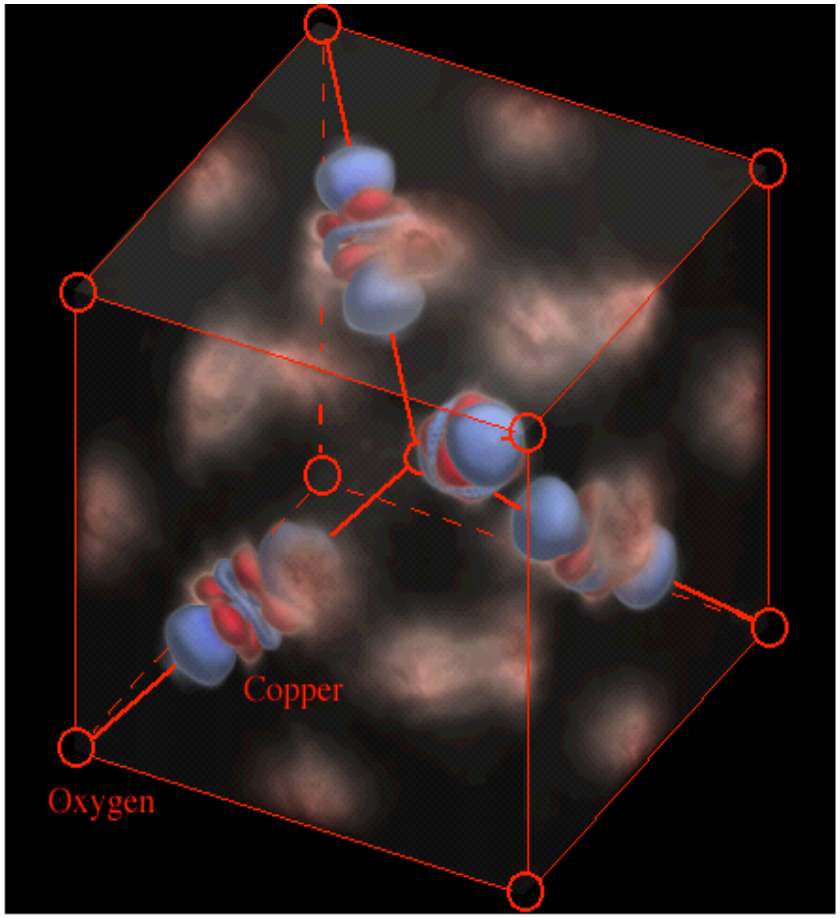

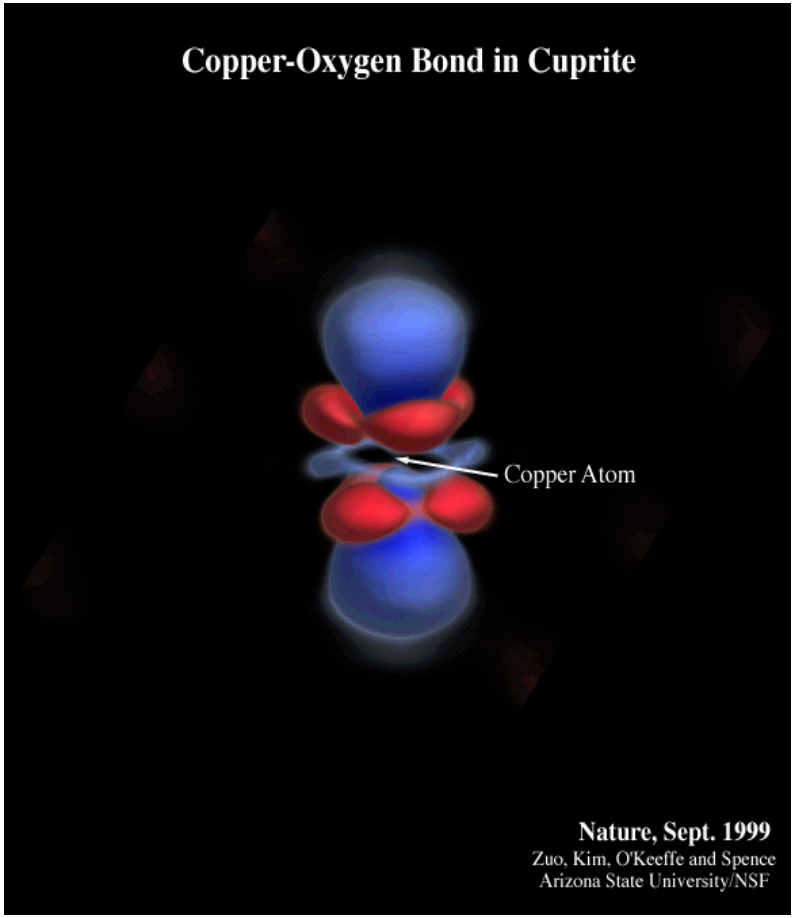

Measured surfaces of constant charge density difference in Cu2O (cuprite). Blue shows less charge than MCDF ions (producing "holes" in the shape of dz^2 orbitals), red is more. Note metal-metal bonds at center of copper tetrahedra. (The coppers form an FCC lattice). If cuprite were purely ionic (Cu+O--) this picture would be blank. Image clearly shows deviation from ionic bonding, e.g the dz^2 hole and co-valent metal-metal bonding. About 0.22 electrons of charge have moved from the hole into this bond. This experimental image also shows effects not predicted by FLAPW/LDA theory, such as the copper-copper bonds. Results are sufficiently accurate to distinguish between many-e approxs (LDA, GGA).

Electron SF very sensitive to ionicity

*Zuo, Kim, O"Keefe, Spence, Nature, 401, p.49 (1999)

Diffuse electron scattering is intense, giving model for phase-transitions.

The atomic mechanism of metal-insulator phase transition in Magnetite*

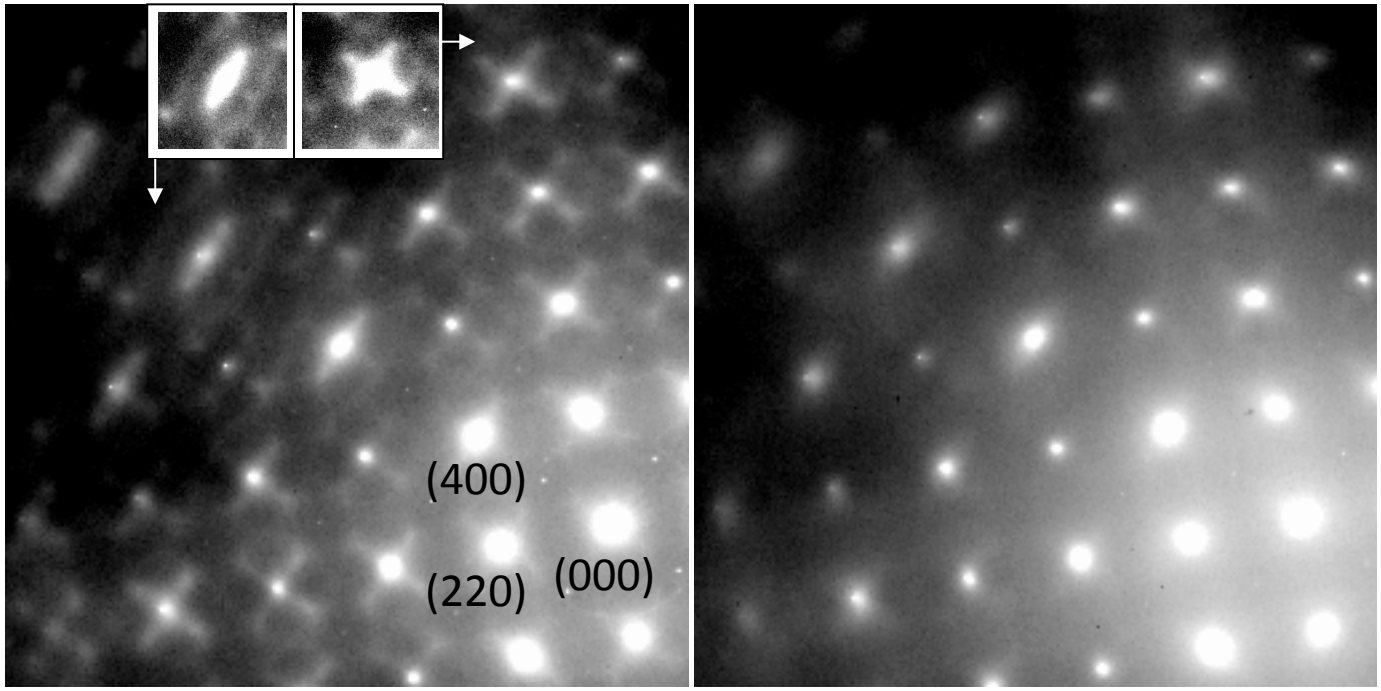

Diffuse scattering in Magnetite at metal-insulator Verwey transition (about 120K).
a) 130K b) 326 K. Inset: (800) left (880) right.

Elastically filtered scattering recorded using Image Plates. (Leo Omega 912).

*Zuo, Pacaud, Hoier, Spence. Micron, 31, p. 527 (2000).

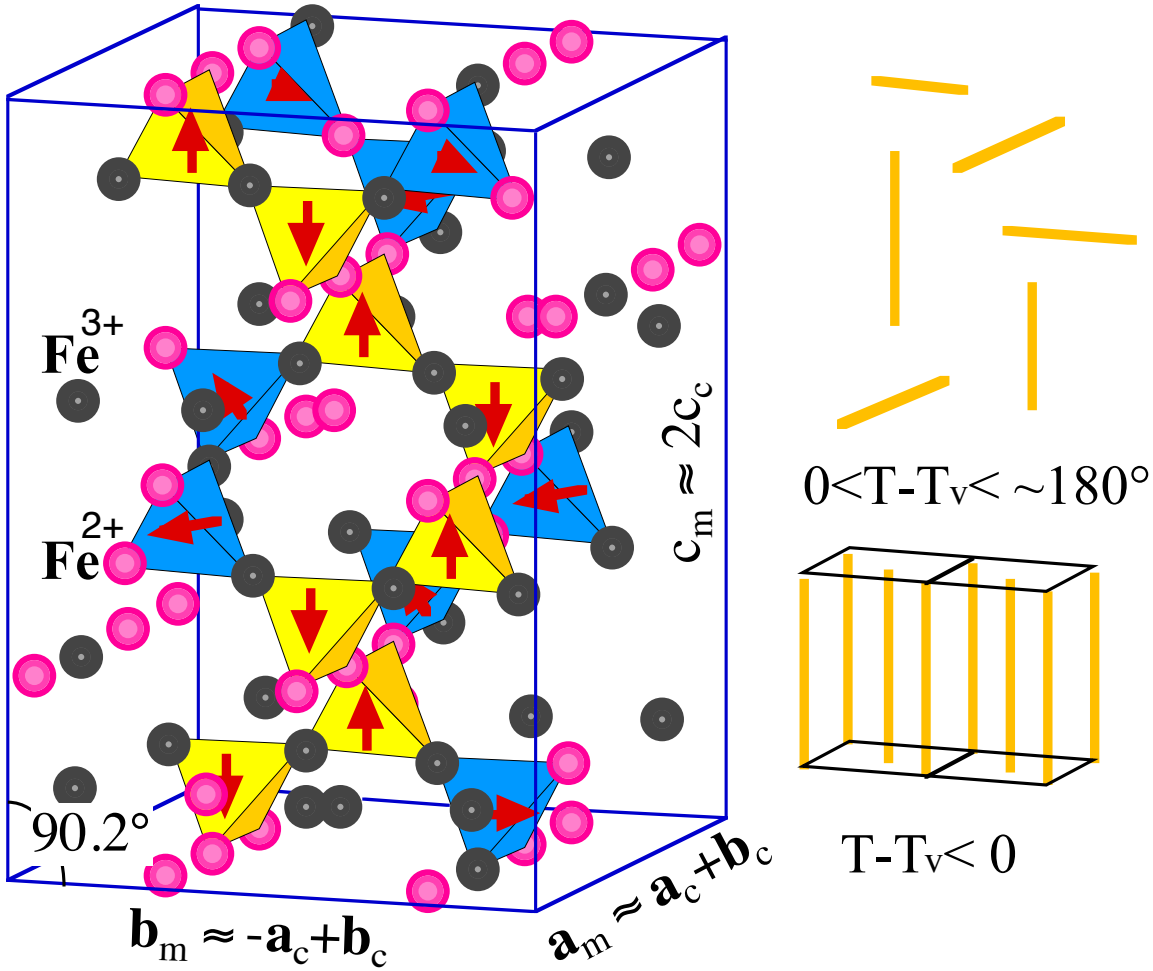

The monoclinic cell of our low temperature charge ordering model (model 2, B-sites only). The yellow tetrahedrons (molecular polarons) form a linked chain with alternating opposite dipoles (red arrows). The chains are separated by molecular polarons of different orientations (blue). The left shows the schematic arrangement of the spiral chains (shown as bars) above and below Verwey transition.

The flipping method has been extended to powder diffraction

1. How can a three-dimensional charge-density possibly be obtained from 1D data ?
2. The patterns can be indexed, Bravais lattice found. This gives a 3D reciprocal lattice to weight with Structure Factor magnitudes and phases. (then phasing problem is as for single xtal, whose reflns are symmetry merged)
3. Last problem is overlaps 1. Accidents - 511, 333 ; 2. Limited angular resolution.
4. To partition overlapping reflections in the flipping algorithm, iterate with complex estimate of F_{hkl}, unlike previous methods -

Experimental ring intensity

Previous estimate

$$F'_k(h) = \frac{|F_{obs}(h)|}{|\langle F_{calc}(h)\rangle|} F_k(h)$$

Current estimate of ring intensity

New estimate
at one reciprocal lattice point

Previous algorithms (Le Bail) use
|F' | = (|Fob|/|Fav|) * |F|

We weight previous estimate by ratio of experimental average to average of current estimates to get new value

Wu et al Nature Materials 5, 647 (2006)

Different structure factors on the same ring are separated by flipping

Pyrite
FeS_2

cubic

Note separation of degenerate reflections in this cubic system

Table 1 List of moduli of Bragg reflections obtained by Fourier transform of the reconstructed structure at iteration 125 ($|F_{125}(h)|$), calculated from refined pyrite structure ($|F_{sim}(h)|$), and obtained from the measured modulus from powder diffraction data ($|F_{av}(h)|$). For the last three columns the scale is the same and set to $|F_{av}(h)|$.

hkl	2θ (°)	$\|F_{125}(h)\|$	$\|F_{sim}(h)\|$	$\|F_{av}(h)\|$
511	95.25	3.70	4.78	3.92
333	95.25	2.42	3.51	3.92
320	61.67	0.08	0.00	2.80
230	61.67	4.83	3.54	2.80
210	37.07	5.04	3.52	2.53
120	37.07	0.09	0.00	2.53
600	117.08	0.72	1.25	1.67
442	117.08	1.68	3.02	1.67
420	78.96	2.24	2.83	2.82
240	78.96	2.31	2.83	2.82
520	99.92	0.08	0.00	1.25
250	99.92	1.13	1.43	1.25
432	99.92	0.18	0.12	1.25
342	99.92	2.17	2.77	1.25
321	64.27	4.13	2.62	2.02
312	64.27	2.29	1.47	2.02

Removal of multiple-scattering artifacts.

Dynamical inversion

1. Spence, Calef and Zuo HIO

2. Dynamical Ptychography – see Electron Centenary book

3. Two-wavelength method for soft Xrays. *Does absorption kill it off ?*

4. With Les Allen – images at two thicknesses.

5. Method of C. Koch – Polynomial solution of Moodie.

The LCLS is the world's first hard X-ray laser

First lasing in April 2009. The LCLS at Stanford is the world's first hard X-ray laser. It produces 9 kV X-rays (1.4 Ang) in 5 - 200 fs pulses, about 1E12 photons per pulse.

Experimental geometry

AIMS:

OUTRUN DAMAGE ? Currently PX limited by damage and xtal quality.
SOLVE SUBMICRON ("invisible") XTALS ?
REAL-TIME SNAPSHOT CHEMISTRY AT ROOM TEMPERATURE ?
PUMP-PROBE WITH VERY HIGH TIME RESOLUTION.
SOLVE PHASE PROBLEM ?
SINGLE-PARTICLE IMAGING
Image bond formation ?

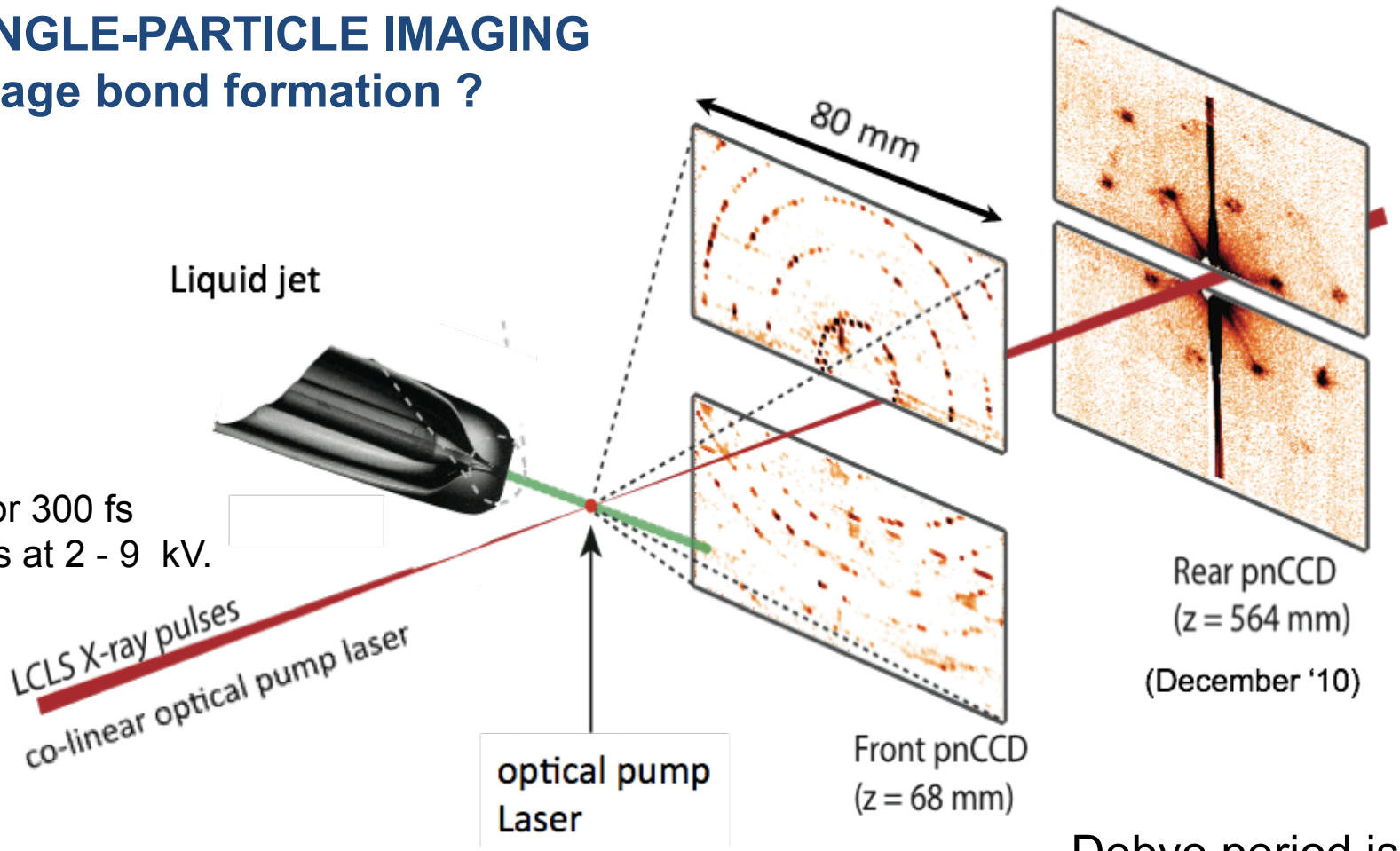

Debye period is ~100fs

The quality and resolution of PX data is limited by *damage* and *crystal quality*.

We use fs LCLS pulses not to get good time resolution, but to outrun damage.

Protein nanoxtals may be more perfect than large xtals. (von Dreele)

Thus sFX breaks the nexus between xtal size, resolution and dose.

Use of short pulses instead of freezing to avoid damage allows RT analysis in liquids, hence snapshot imaging of chemical processes in solution.

But there is no goniometer ! Our Monte-Carlo method assumes there will be a nanoxtal in every orientation needed to integrate over the rocking curve.

Types of experiments:
Nanoxtals, Single particles, Fast WAX, Toothpaste, Mixing jet, 2D xtals, fiber diffraction

Chapman, Fromme……..Spence. Nature 2011

Hydrated particle delivery

Our Liquid jet uses gas focusing to make a micron jet from bigger nozzle.

Gas focusing prevents clogging - get *submicron droplets* from a 15 micron nozzle
Absence of fields (electrospray) prevents charge artifacts on proteins.
Liquid feed ! No goniometer !

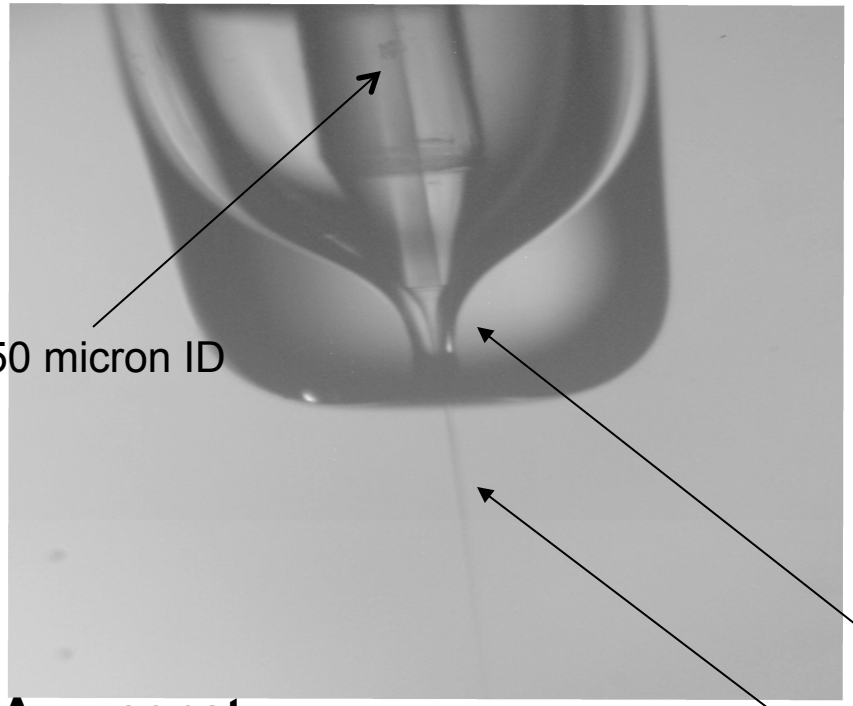

Uwe Weierstall: Triggered Rayleigh jet

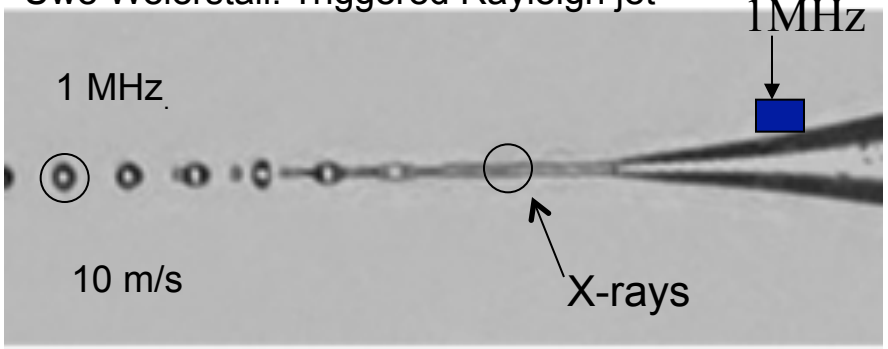

LCLS Rep Rate ~100 Hz
Droplet frequency 1 MHz. v = 10 m/s
Droplet diam 1 micron
LCLS beam diam 1 micron.
Flow rate F= 10 microL per minute. v = F/A

Liquid cone enhances flow alignment
(from HPLC syringe pump)

~1 MHz single-file micron-sized droplet beam. Big nozzle makes Small droplets

Av = const
Gas accelerates liquid
Making cone as shown.
Higher pressure for smaller droplets

Allows study of *irreversible* processes in *fully hydrated* biomolecules

M. Frank, Mike Bogan, have gas-phase jet

Agilent, Medical Rayleigh 1890

Spence, Doak, Phys Rev Letts. 92, 198102 (2004). Weierstall, Doak, Spence Rev Sci Instr. (2012)

Liquid jet sample delivery system.

Pump-probe in a jet – first trials of time-resolved PX for *irreversible* processes.

New ASU jet for June 2010 had microscope, retract nozzle, pump laser

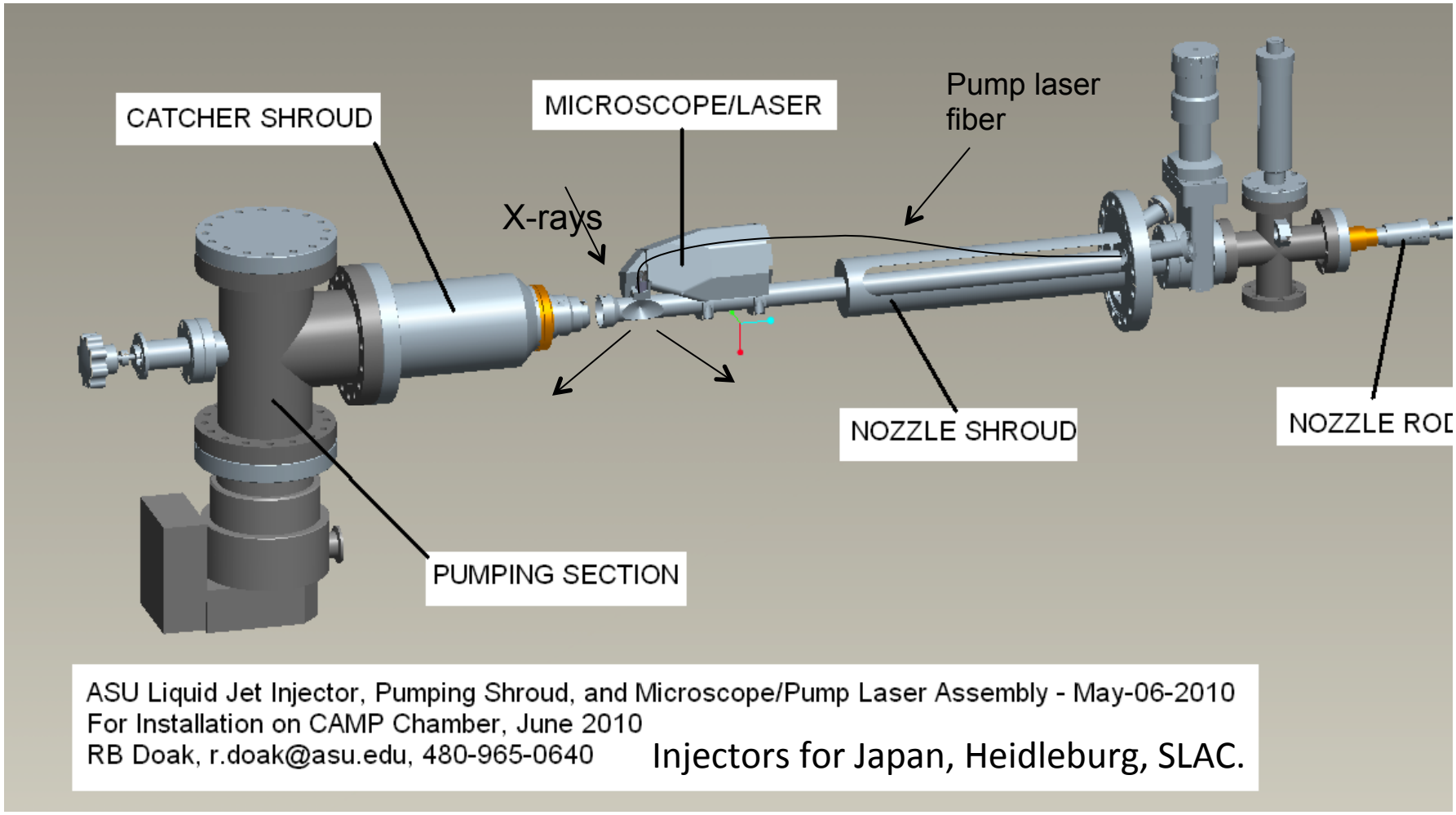

Injectors for Japan, Heidleburg, SLAC.

Femtosecond pulses are use to avoid radiation damage, not to give good time resolution

Droplets freeze in vacuum at 10^6 $^oK/s$

Doak, Weierstall, Spence

We can sum the Bragg spots as they arrive (virtual powder pattern)

Lysozyme, 1.8 kV.
6.9 Ang wavelength

With 6 x10^6 patterns, human examination of the data is impossible !

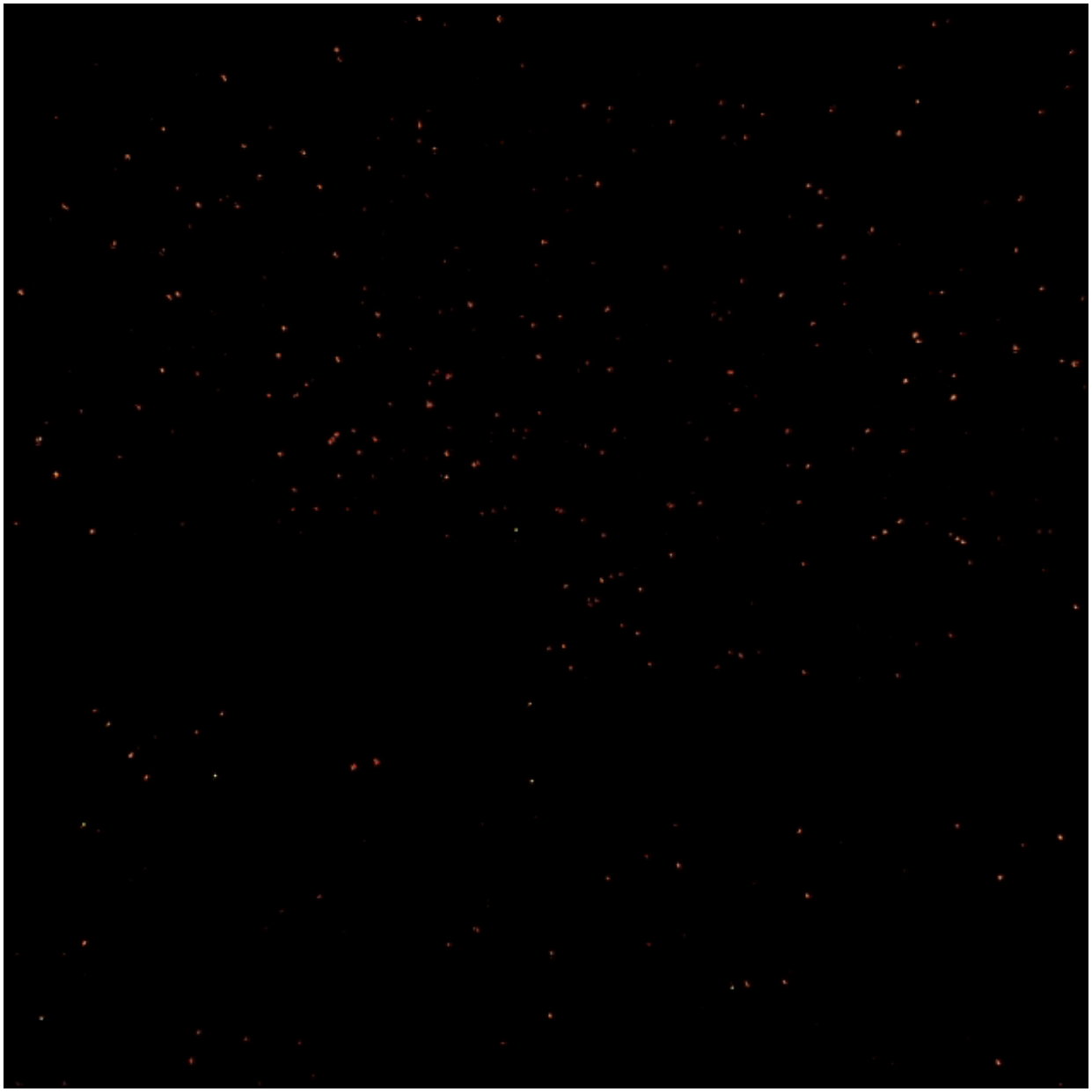

Each 2kV shot is 70 fs, 2 mJ
1E12 photons per shot
900 J cm^{-2} fluence
1E16 W/cm^2
7 micron diam beam
Dose 700 MGy per pulse

Ilme Schlichting, Bob Shoeman et al

Shape-transform effects. PSI nanoxtals at 2 kV, random orientation.

In XRD the Ewald sphere takes a SLICE through the 3D FT of the nanoxtal shape
The structure factors are proportional to the VOLUME of the shape-transform.

Confuse autoindexing programs !

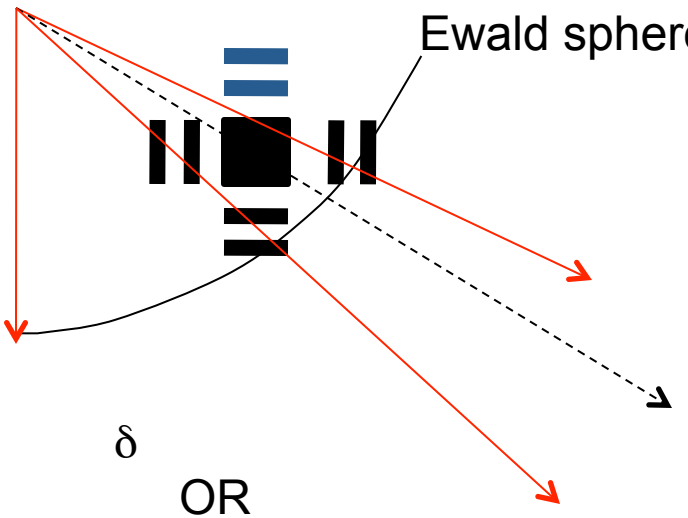

δ

OR

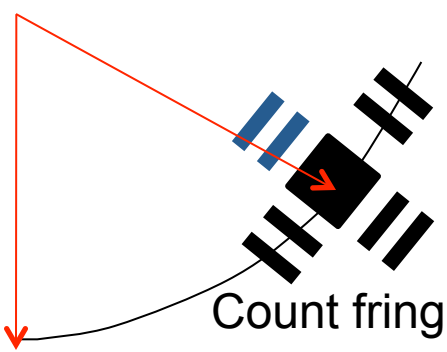

Count fringes to get size

No scattering
in this Bragg direction

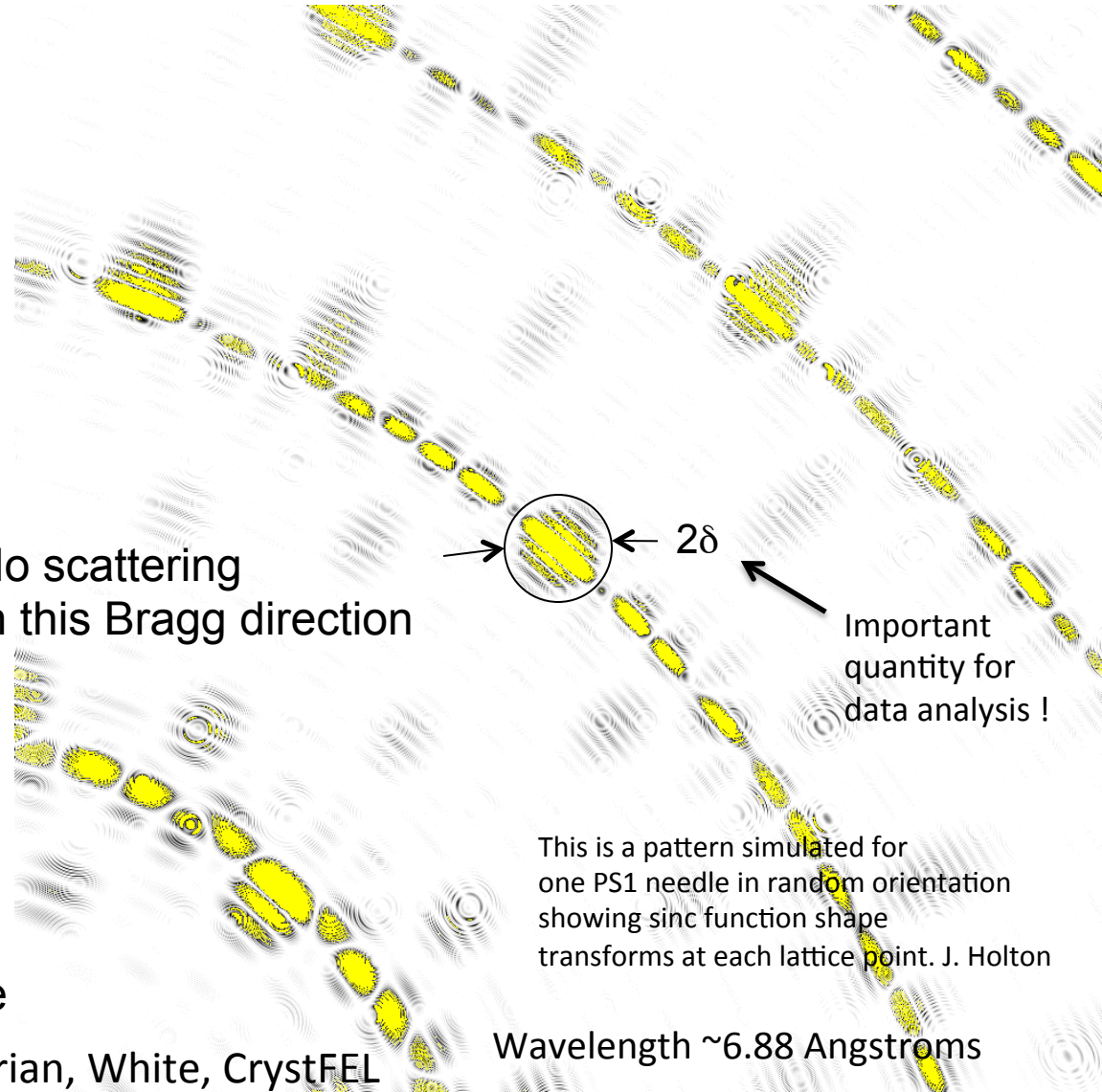

Important
quantity for
data analysis !

This is a pattern simulated for
one PS1 needle in random orientation
showing sinc function shape
transforms at each lattice point. J. Holton

Wavelength ~6.88 Angstroms

Kirian, White, CrystFEL

Milestones

1. Can "diffract-and-destroy" (sFX) give atomic resolution ?

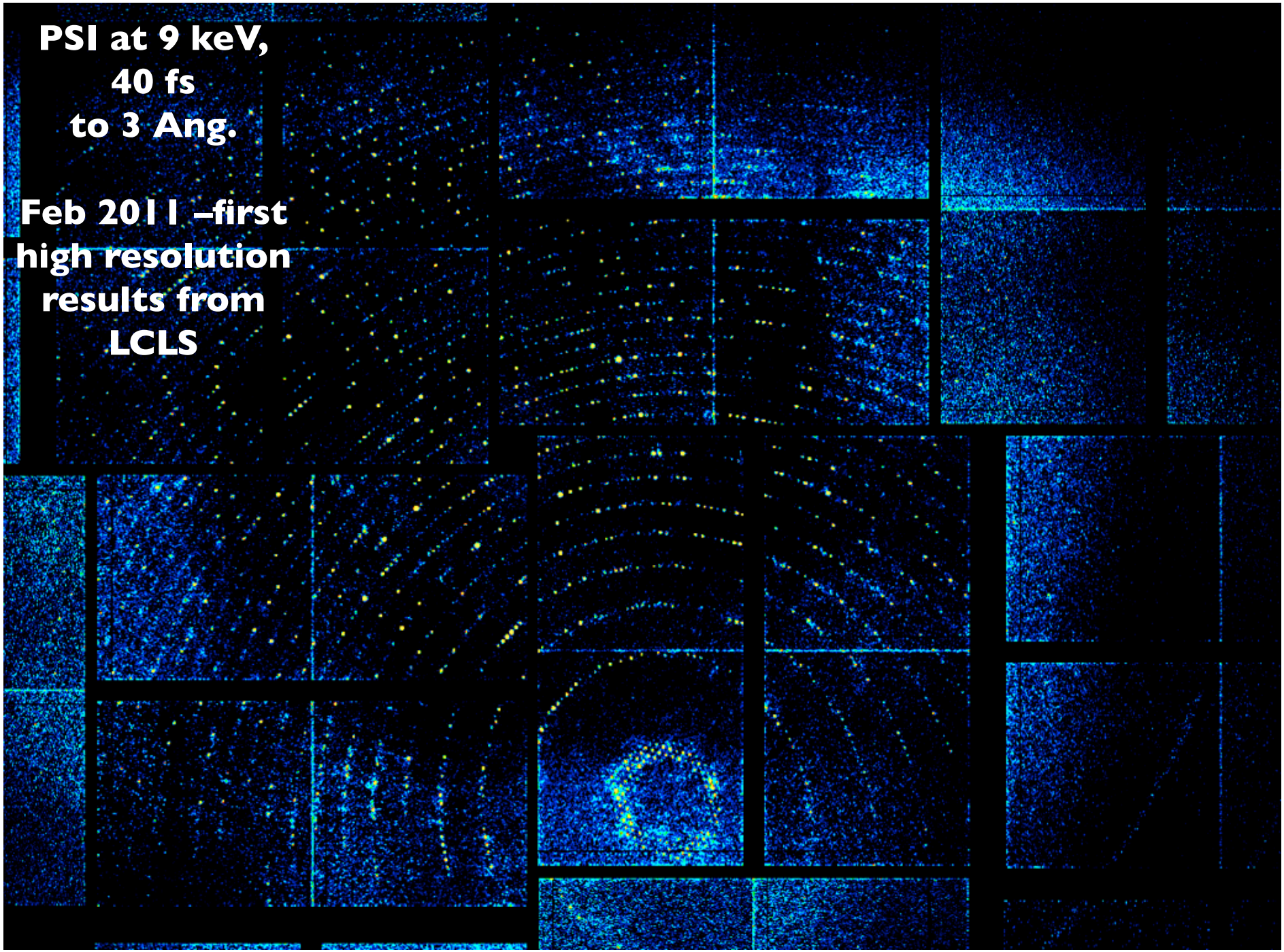
PSI at 9 keV,
40 fs
to 3 Ang.
Feb 2011 –first
high resolution
results from
LCLS

Can diffract-and-destroy give atomic resolution ?

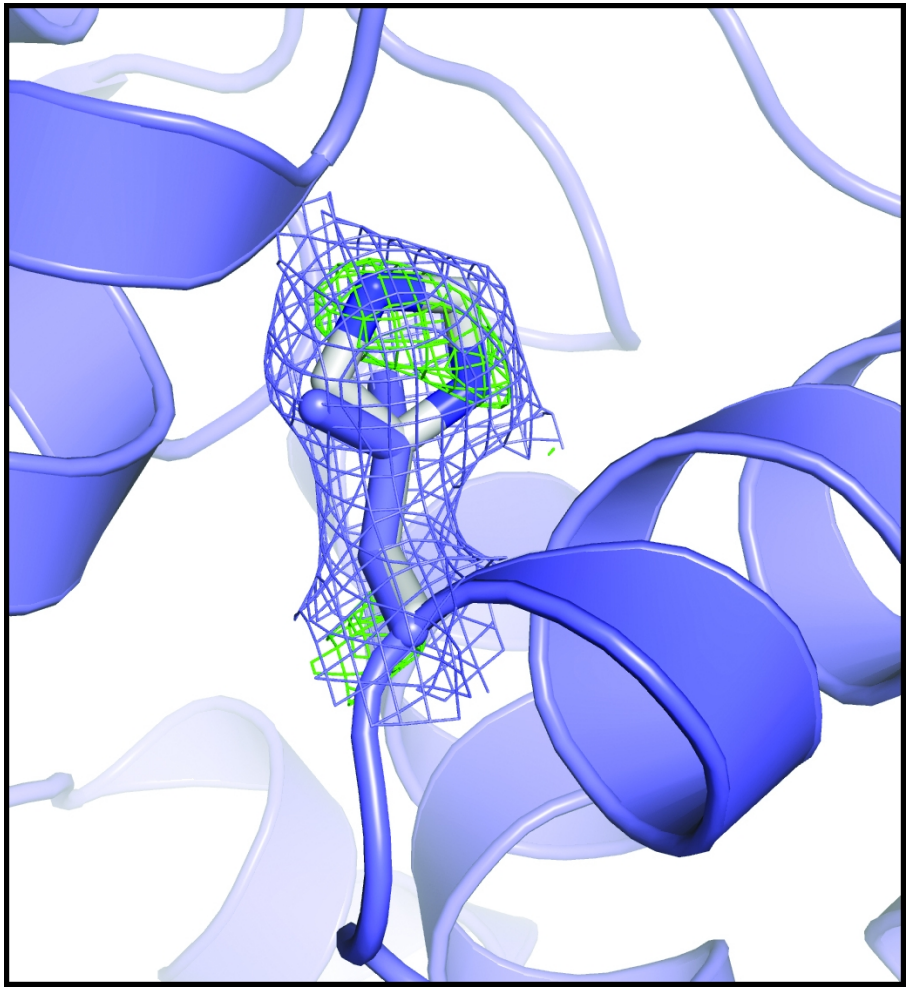

Fig. S3

Quality of the molecular replacement map. The region around Leu15 in the turkey egg white lysozyme model (blue carbon atoms) is shown. In the actual hen egg white lysozyme structure obtained of the presented SFX data, this is a histidine (white carbon atoms). Both the $2mF_{obs}$-DF_{calc} (blue, 1.5 σ) and Fobs-DFcalc (green, +/- 3 σ) maps *(10)* clearly show the difference between the search model and the actual structure obtained from the SFX data.

XFEL data can distinguish Turkey from Hen.

Hen Lysozyme, 1 x 1 x 3 microns xtallites at 9.4 kV with 40 fs pulses, Dose 33 Mgy.
CrystFEL . **RESOLUTION 1.9 ANGSTROMS**.

Serial Femtosecond Crystallography
SFX

Weighted R-factor between LCLS and SLS data is about 10%

D.C.Phillips, L.N. Johnson, 1965
first enzyme solved.

S. Boutet, G. Williams.....I. Schlichting. Science 2012

Milestones

2. Can "diffract-and-destroy" (sFX) give New Biology ?

First new biology at LCLS….'in-vivo" crystallization.

DRUGS FOR SLEEPING SICKNESS affects 60 million
Parasite cells cause Trypanosomiasis, HAT, fatal.
hence drug target.

Knockout of TbCatB is fatal for parasite,

Cathepsin B Enzyme (protease)
Feb 2011. LCLS
Nanoxtals form inside
Sf9 insect cells infected
by baculovirus with CatB DNA.
Not possible by PX.
TbCatB structure needed for rational
drug design of inhibitor to stop
this enzyme doing catalysis.

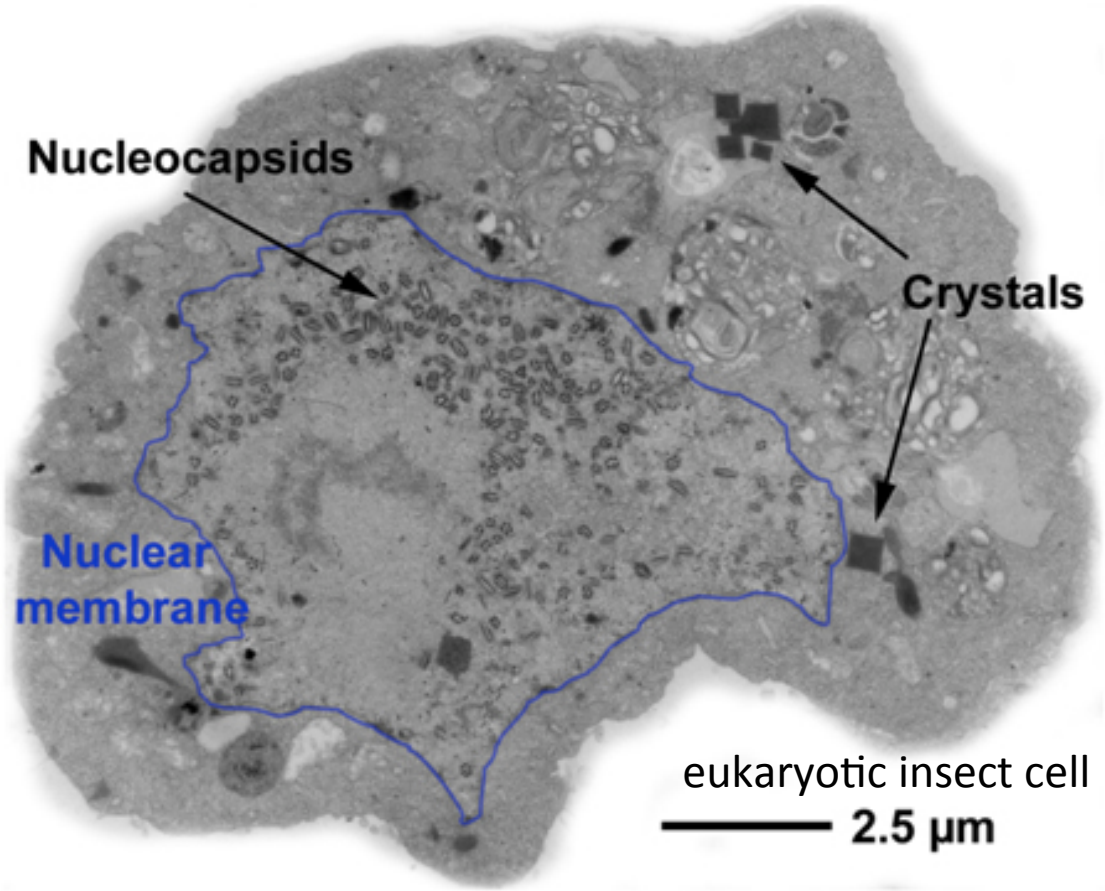

TEM of infected cell,
showing nanoxtals
too small to be solved
by MX .

Koopman, Nass….Duszenko DESY

We have indexed 1.8 Å resolution diffraction from an unsolved glyco-protein, Cathepsin B

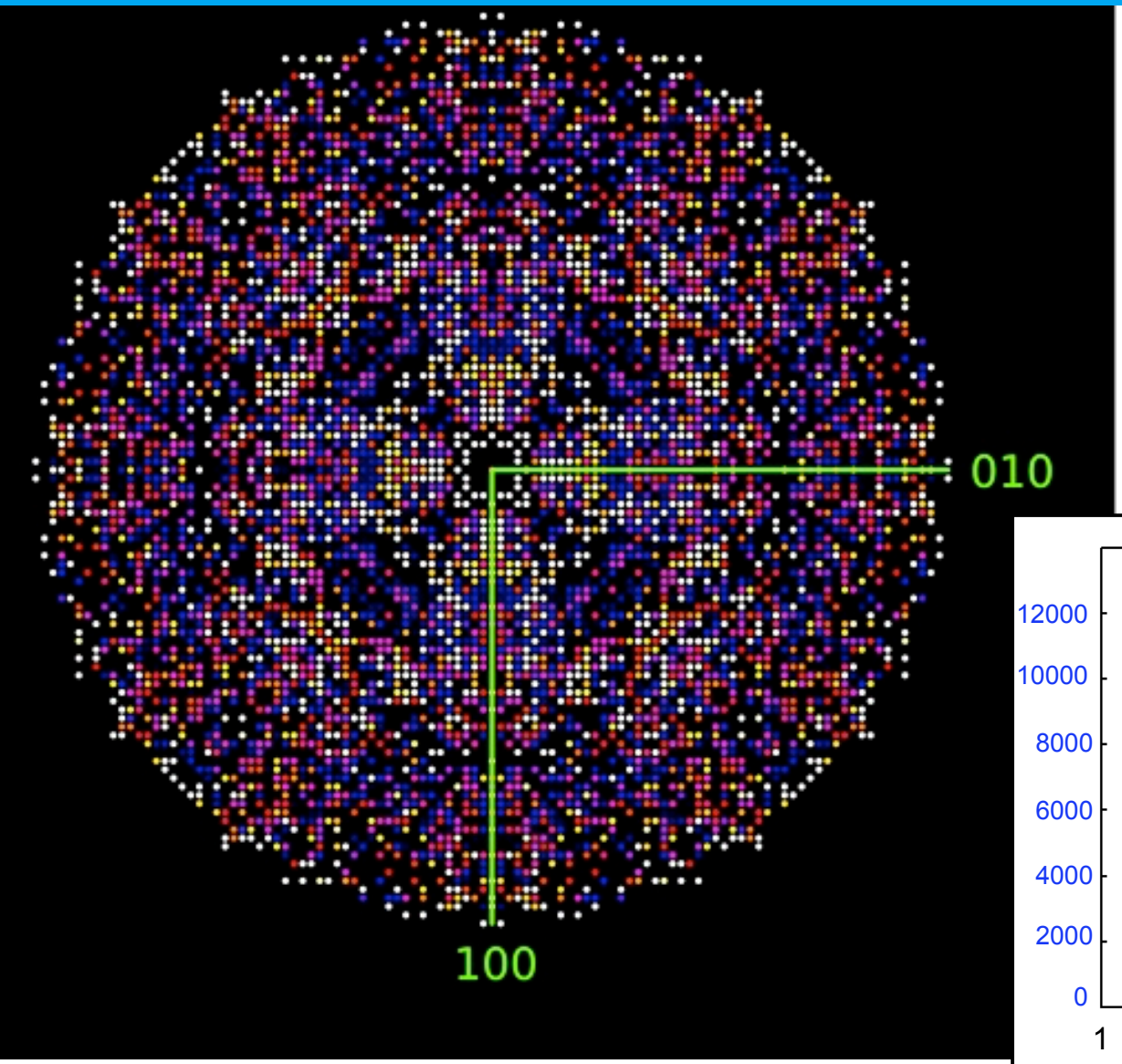

- 3,953,201 frames collected with 40 fs pulses
- 8 hours of data collection
- 357,555 “crystal hits” detected (9%)
- 156,565 indexed (44%)

9 Kv

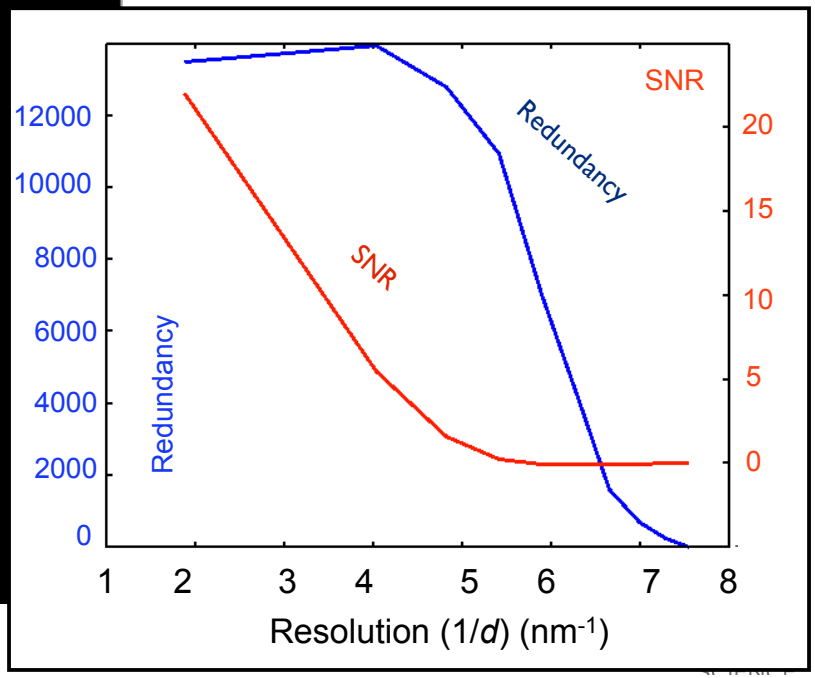

Koopman et al Nature Methods, Jan 2012

Cathepsin B (enzyme) 9 kV
Feb 2011. LCLS
Nanoxtals form inside
Sf9 insect cells infected
by baculovirus (with Cat B DNA).
Eukaryotic cells do post trans mod

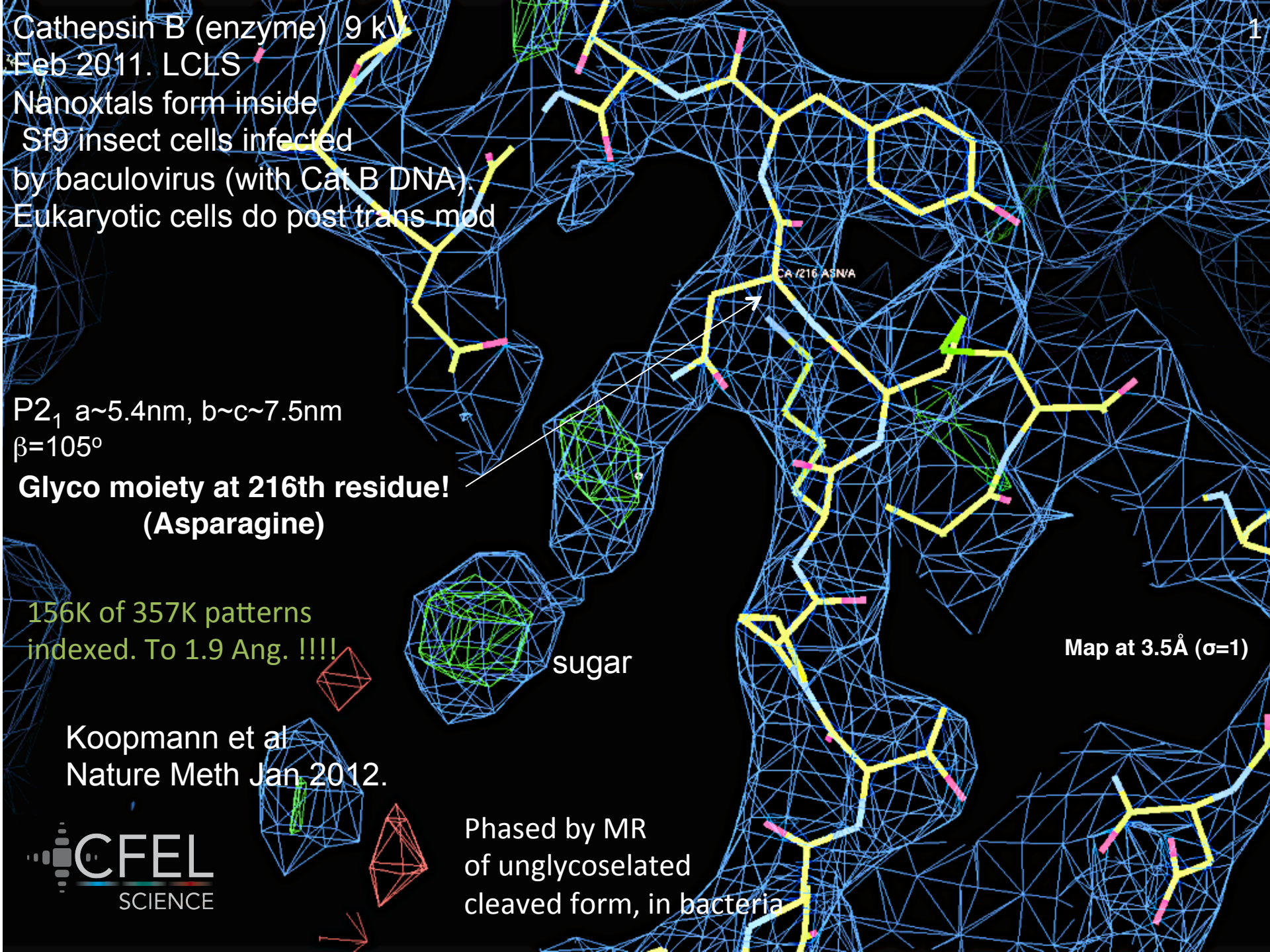

$P2_1$ a~5.4nm, b~c~7.5nm
β=105°

Glyco moiety at 216th residue!
(Asparagine)

156K of 357K patterns
indexed. To 1.9 Ang. !!!!

Koopmann et al
Nature Meth Jan 2012.

Phased by MR
of unglycoselated
cleaved form, in bacteria

CFEL
SCIENCE

The previously-unknown structure is determined to 1.8 Å resolution

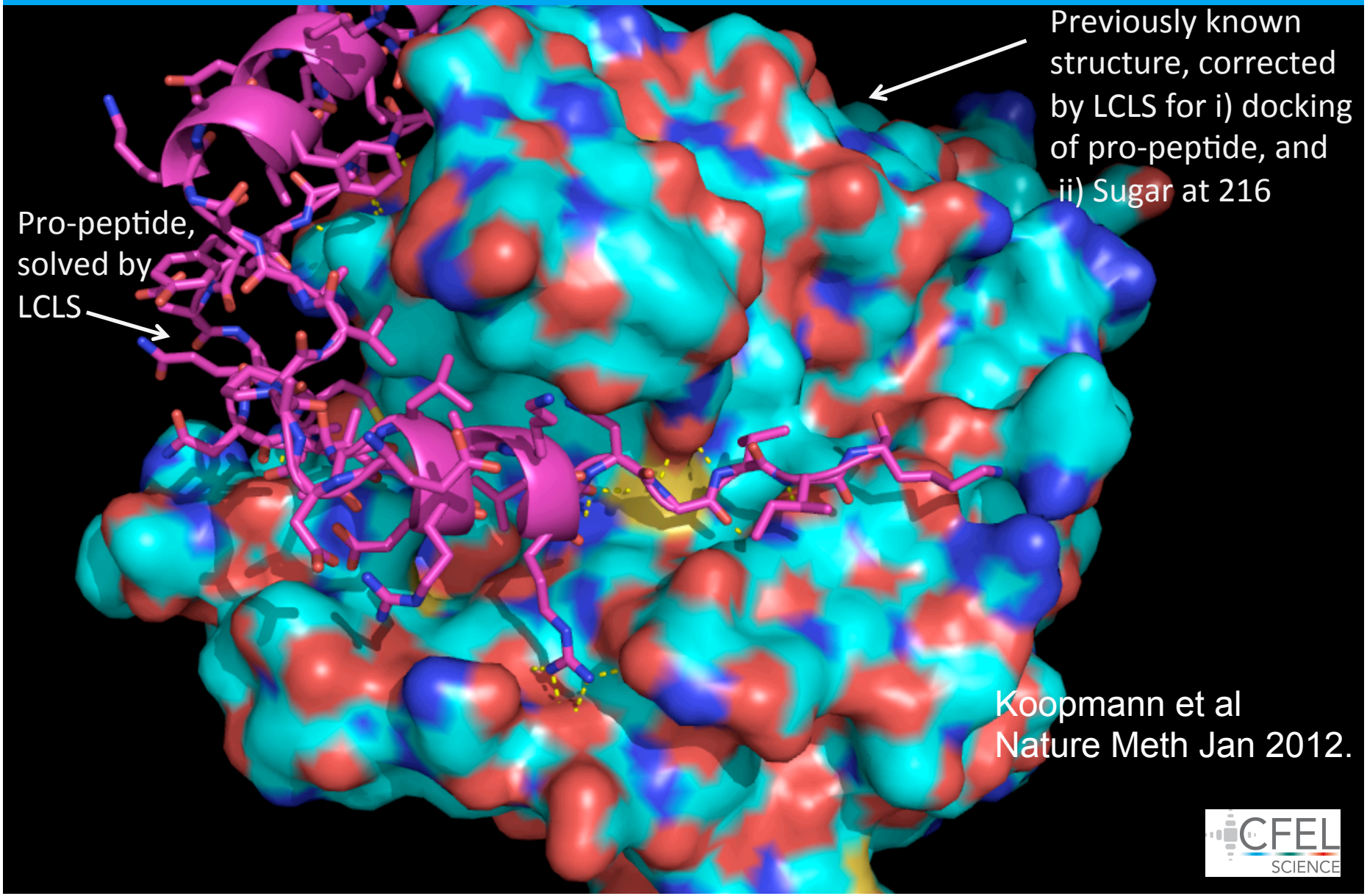

Milestones

3. Time-resolved nanocrystallography : pump-probe in a jet.

Earlier work… Moffat, Anfinrud, Neutze…..

Arrangement for pump-probe time-resolved nanoxtallography in our jet

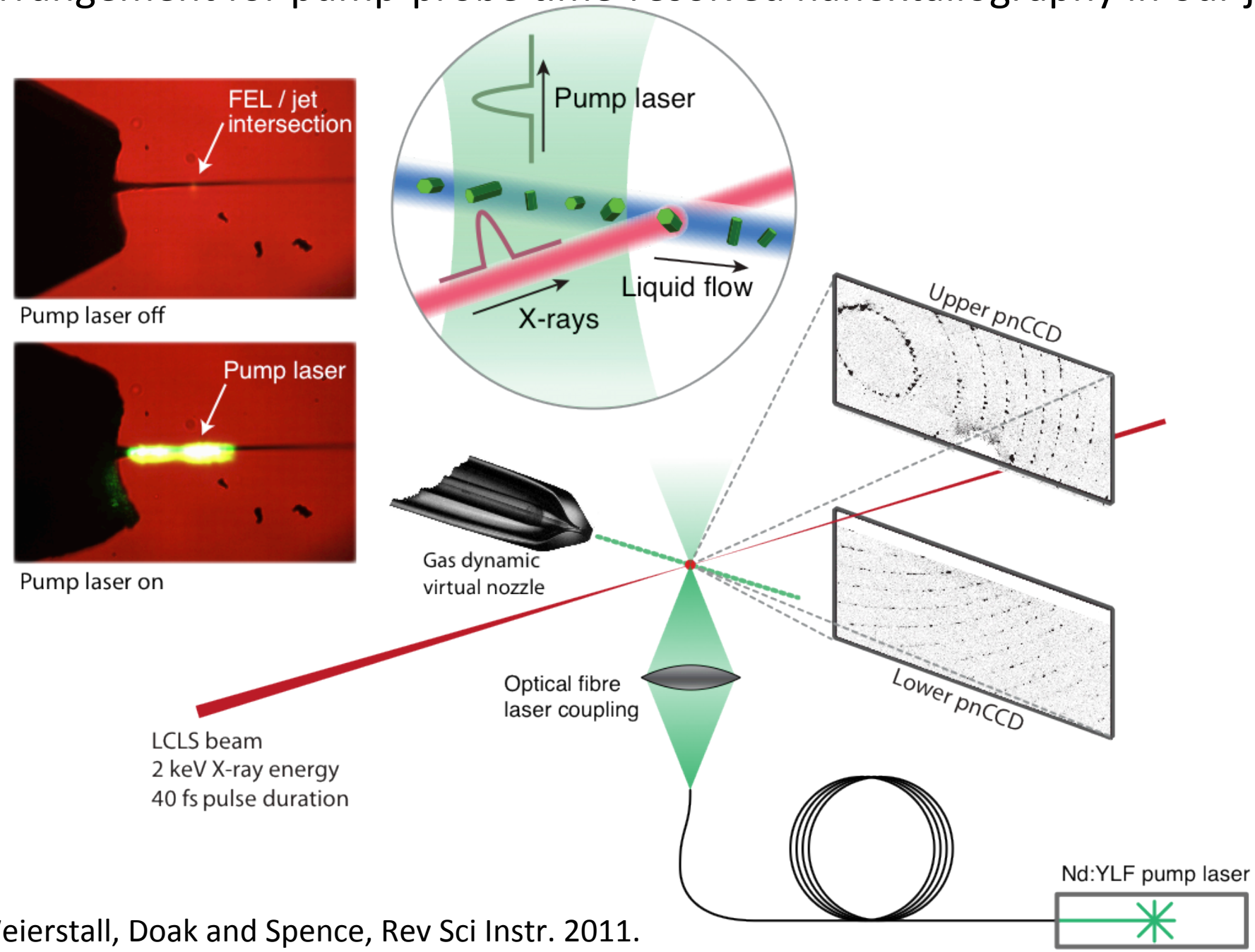

Weierstall, Doak and Spence, Rev Sci Instr. 2011.

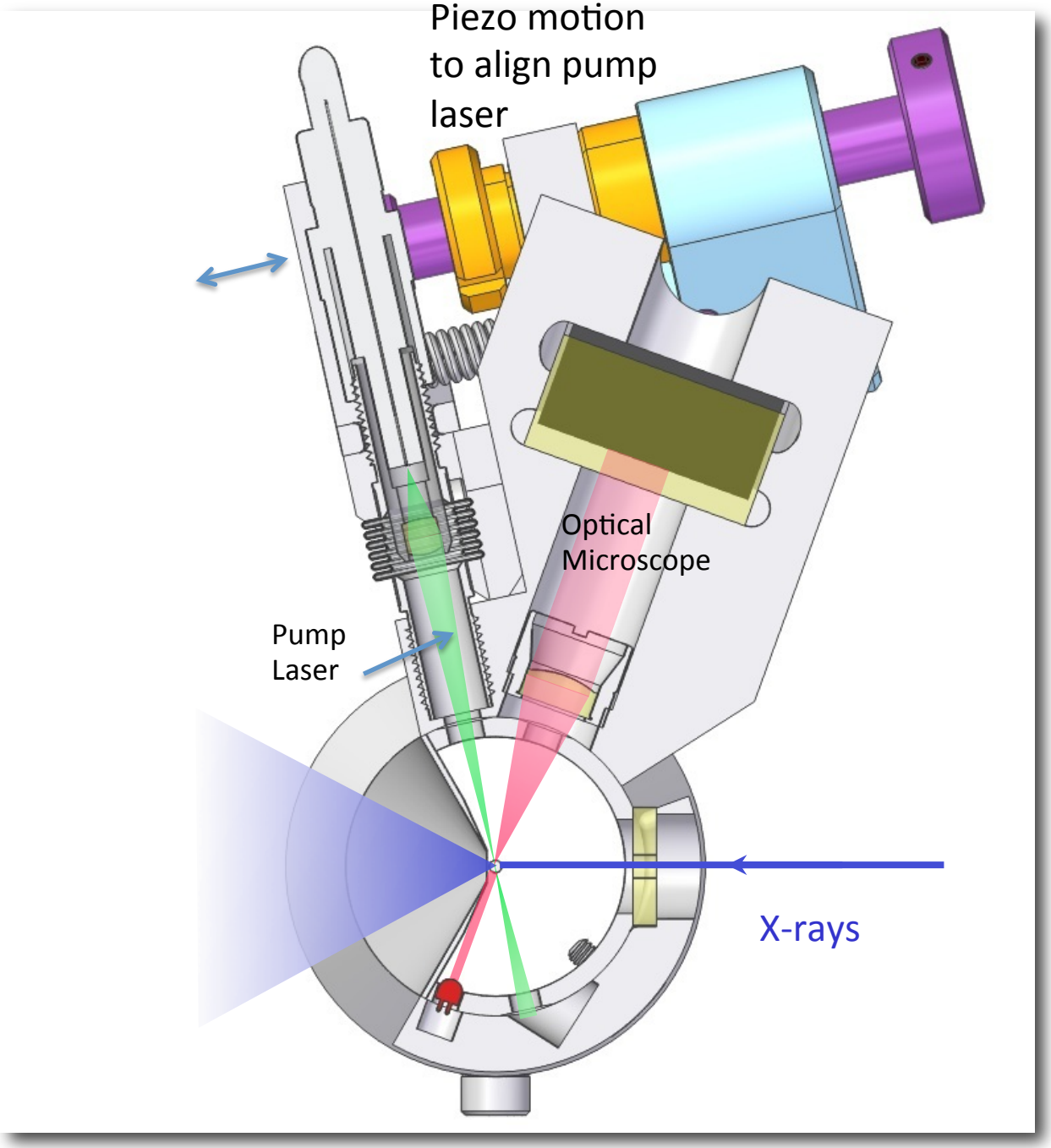

Pump laser for photoexcitation of the sample

Four axes must pass thro a point with submicron precision – X-ray axis, microscope axis, pump laser axis and liquid jet.

The in-vacuum CCD camera allows us to watch mols exploding when aligned.

PHOTOSYSTEM I Ground state. $P6_3$ (sixfold screw along c, advance by half)

Maintains biosphere, Eats CO2. PSII splits water. Generates oxygen. Energy via ATP

CO2 is reduced to carbohydrate

water is oxidized into molecular oxygen.

From cyanobacteria
12 proteins, cofactors

1 MDa

72,000 non-H atoms.
PDB 1JB0

13 years from first microxtals to big xtals , to structure !
Solved in 2001 at 2.5 Ang.

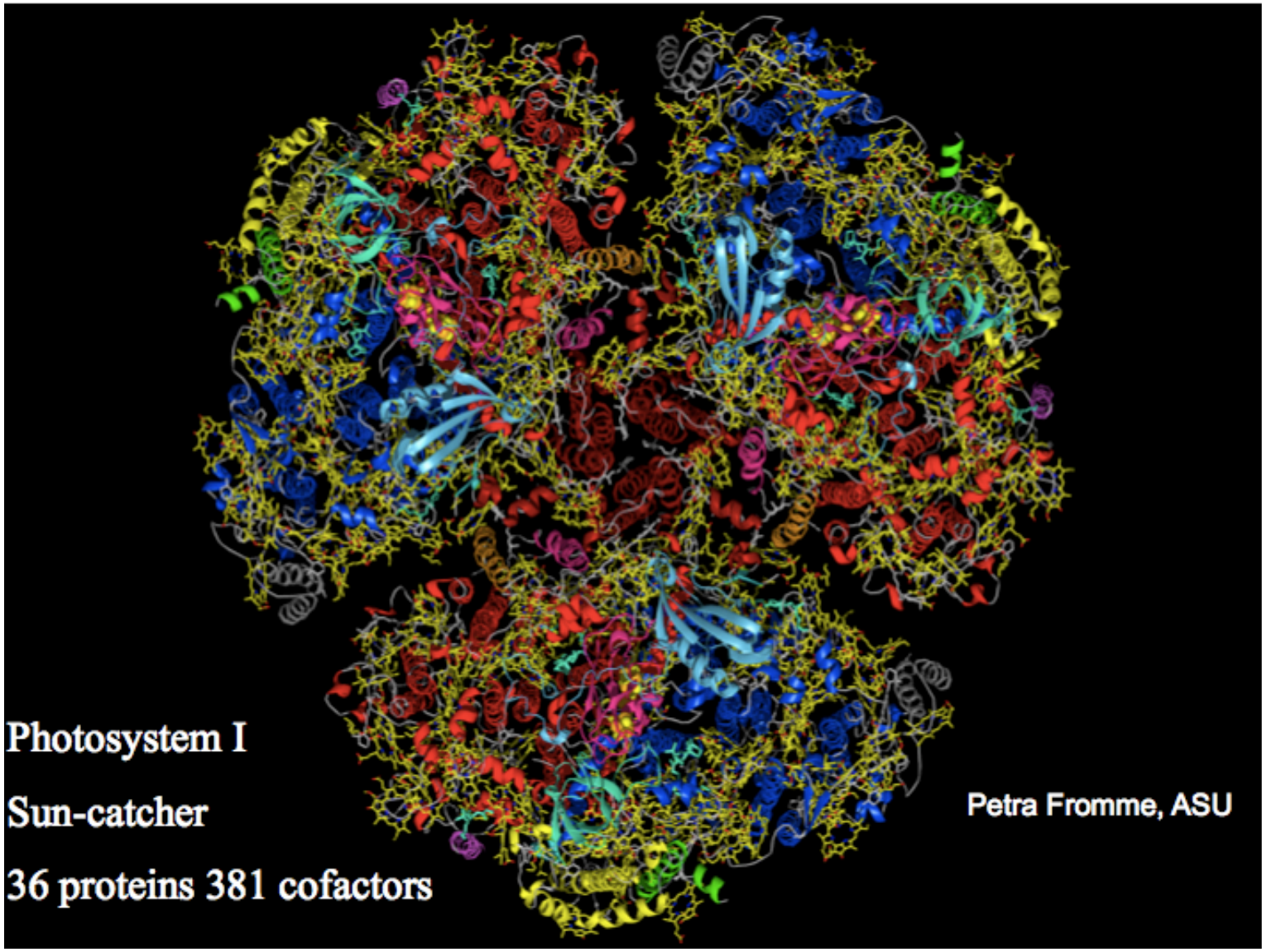

Pump-probe on PSI-ferre co-crystals

captures light at antenna complex, separates charge, prevents photo-damage.

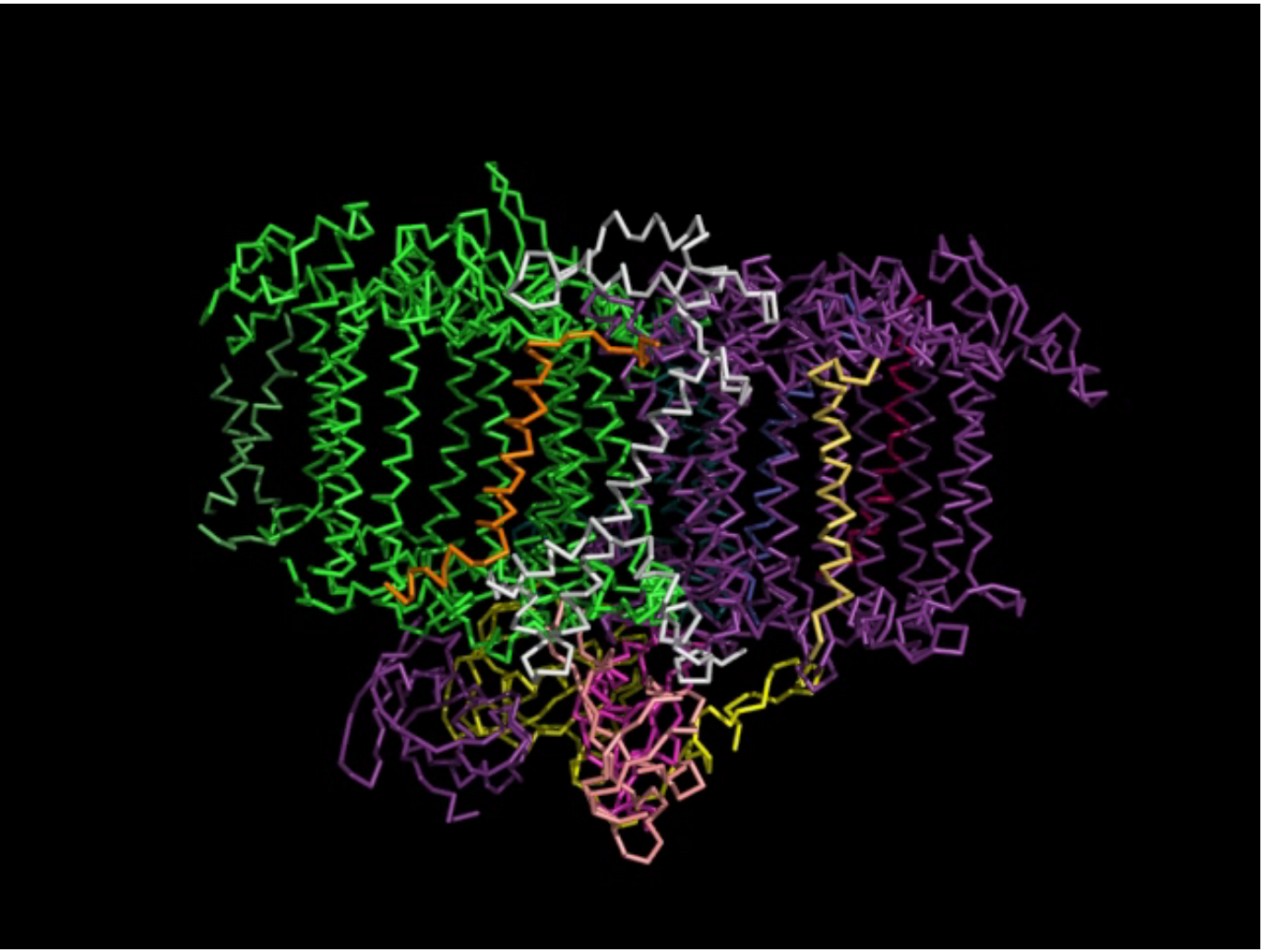

Electron transfer
to ferredoxin causes
undocking and
dissociation of ferre. to FNR

The Fromme group
grew 2 micron PSI-ferre
co-xtals *in the dark*.
(dissolve in light)

Ferredoxin is an e^- carrier
for redox reactions.

Pulsed absorption spectros
shows docking has 3 phases
500ns, 1.5 & 20 microsec.

We use 5,10 microsec to
watch undocking.

Movement of ferredoxin molecule on Photosystem 1 during electron transfer.

Chosen because undocking is irreversible

Mark Hunter et al …

Pump-probe experiments are possible with the liquid jet. PSI-ferre.

Pump laser and XFEL on jet - exploding nanoxtals

Like sunlight on a leaf….snapshots of the excited state density

Movie

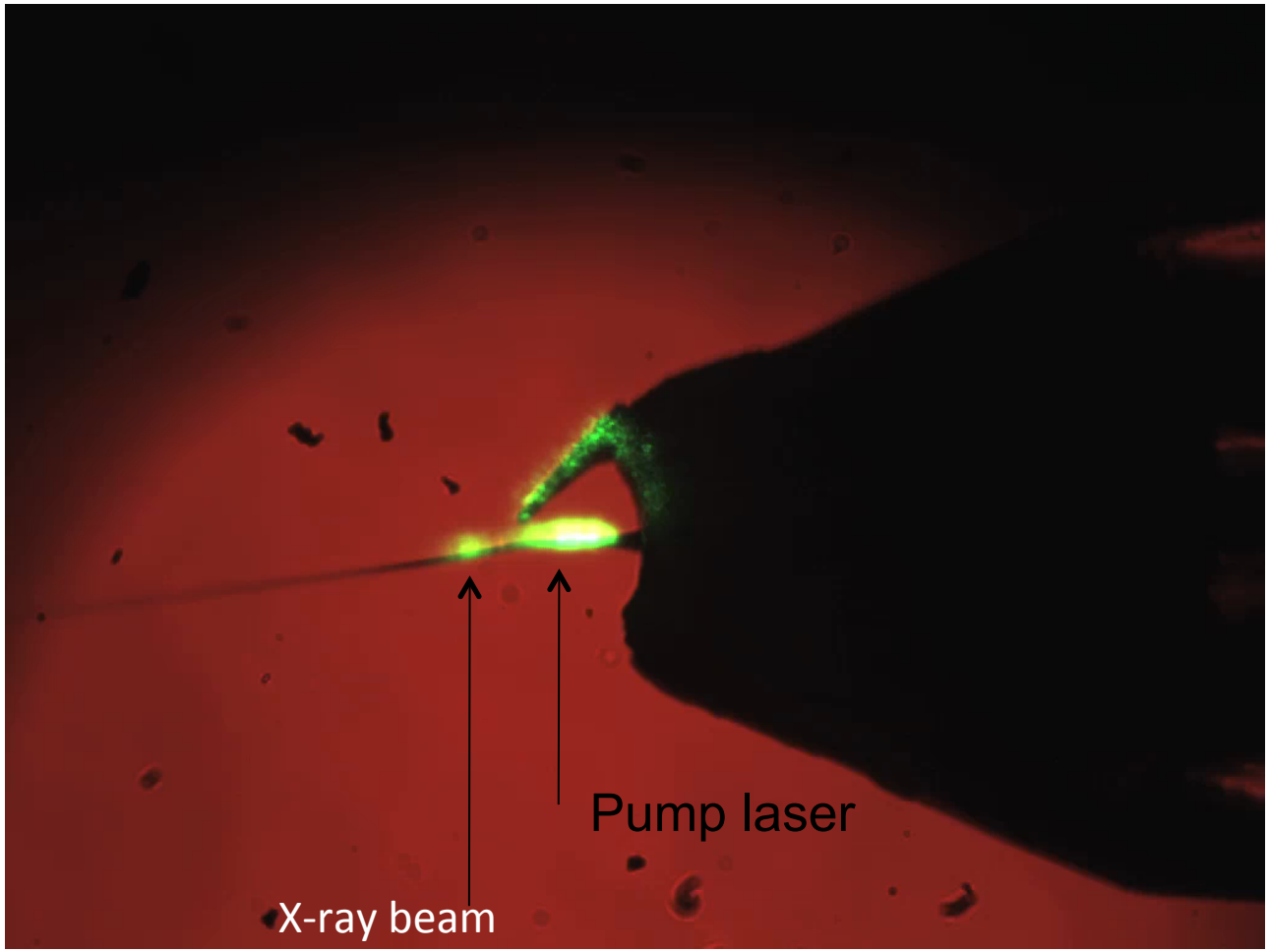

pump laser:
532nm,
7ns pulse, 10 microjoules,
focused to 100 micron spot,
fiber coupled,

Time delay between 70 fs X-ray pulse and laser 0 - 10μs

7 micron beam
2 micron xtals
4 micron jet

To observe undocking of ferredoxin from PSI, excite nanoxtal 10 microseconds before XRD snapshot
Travelling at 10 m/s, nanoxtals go 100 microns, less than width of 400nm doubled Jedai fs beam
Flow rate 10 microliters/min.

Time-resolved pump-probe XRD of ferredoxin undocking from PSI

Electron transfer causes undocking. Ferre is responsible for entire redox regulation in plants. PSI-ferre solved by Fromme at 3.8 A -3KCD

Any LCLS damage effect is the same for all. Irreversible changes

Takes CO_2 to sugar

A. Aquila et al Optics Express 2011

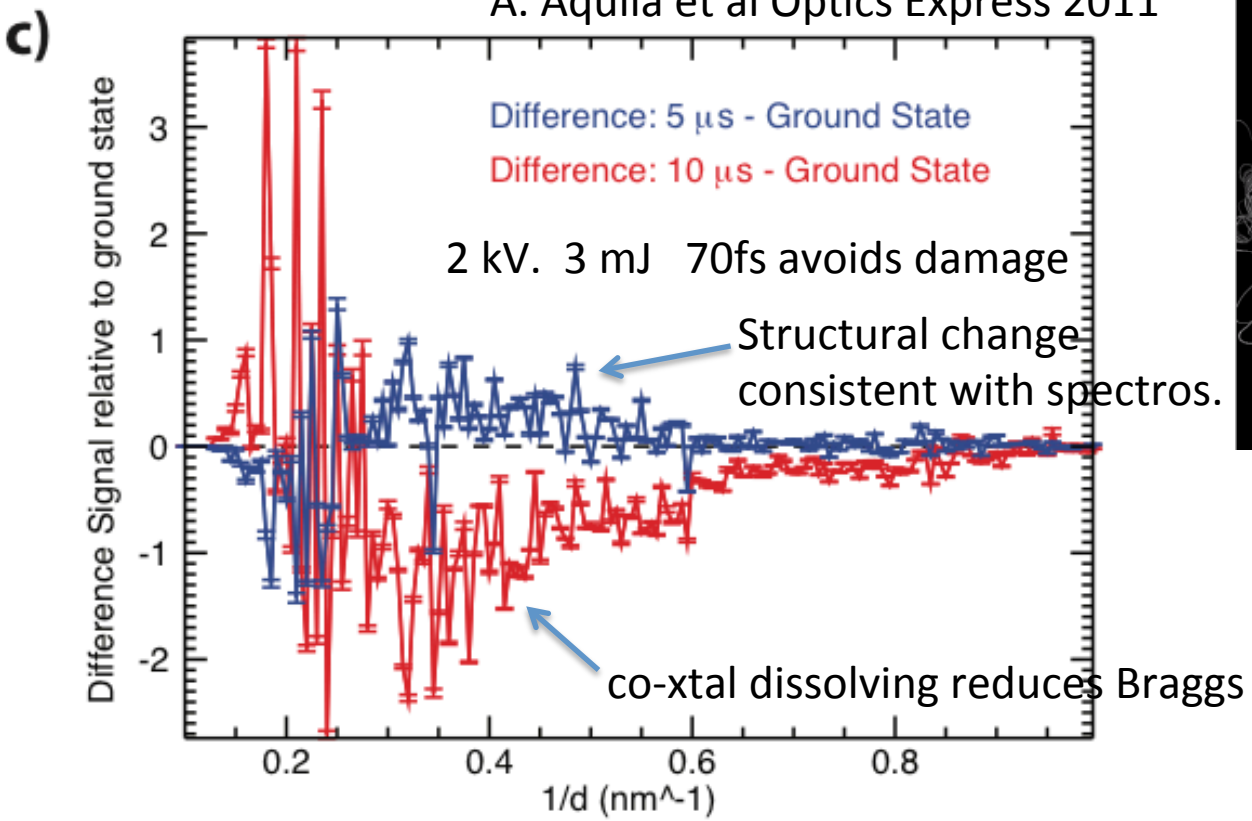

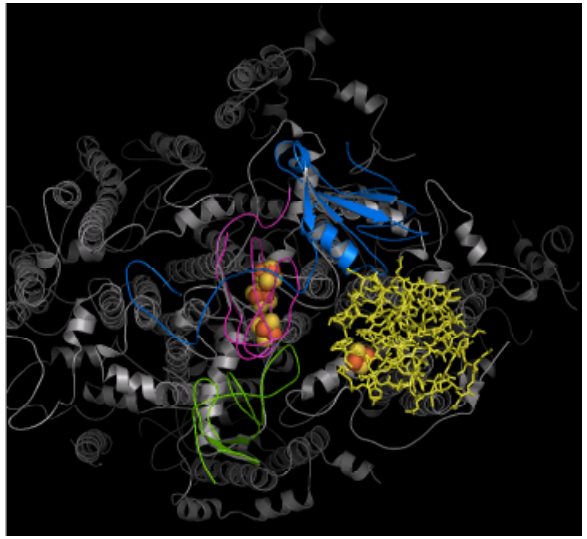

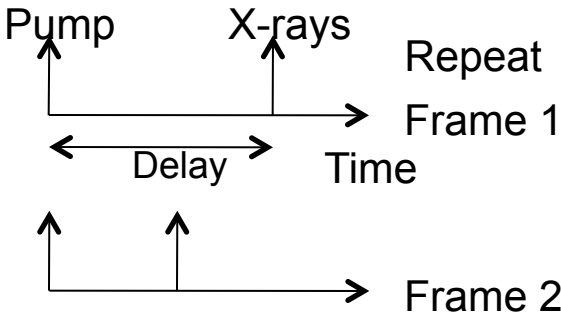

Scaled to minimize RMS difference between virtual powders

219,960 frames at 5 microsec of which 7% indexable

Snapshot structure factors measured for 3 delays between pump laser and 70 fs X-ray pulse. Pump laser causes electron transfer, which causes undocking. Then entire xtal falls apart (but not the mol). Small change in lattice constants consistent with 3deg temp change, up to 10 microsecs, indicating no serious damage.

At longer pulse durations, high order Bragg spots fade

Photosystem I radial average of diffracted intensity

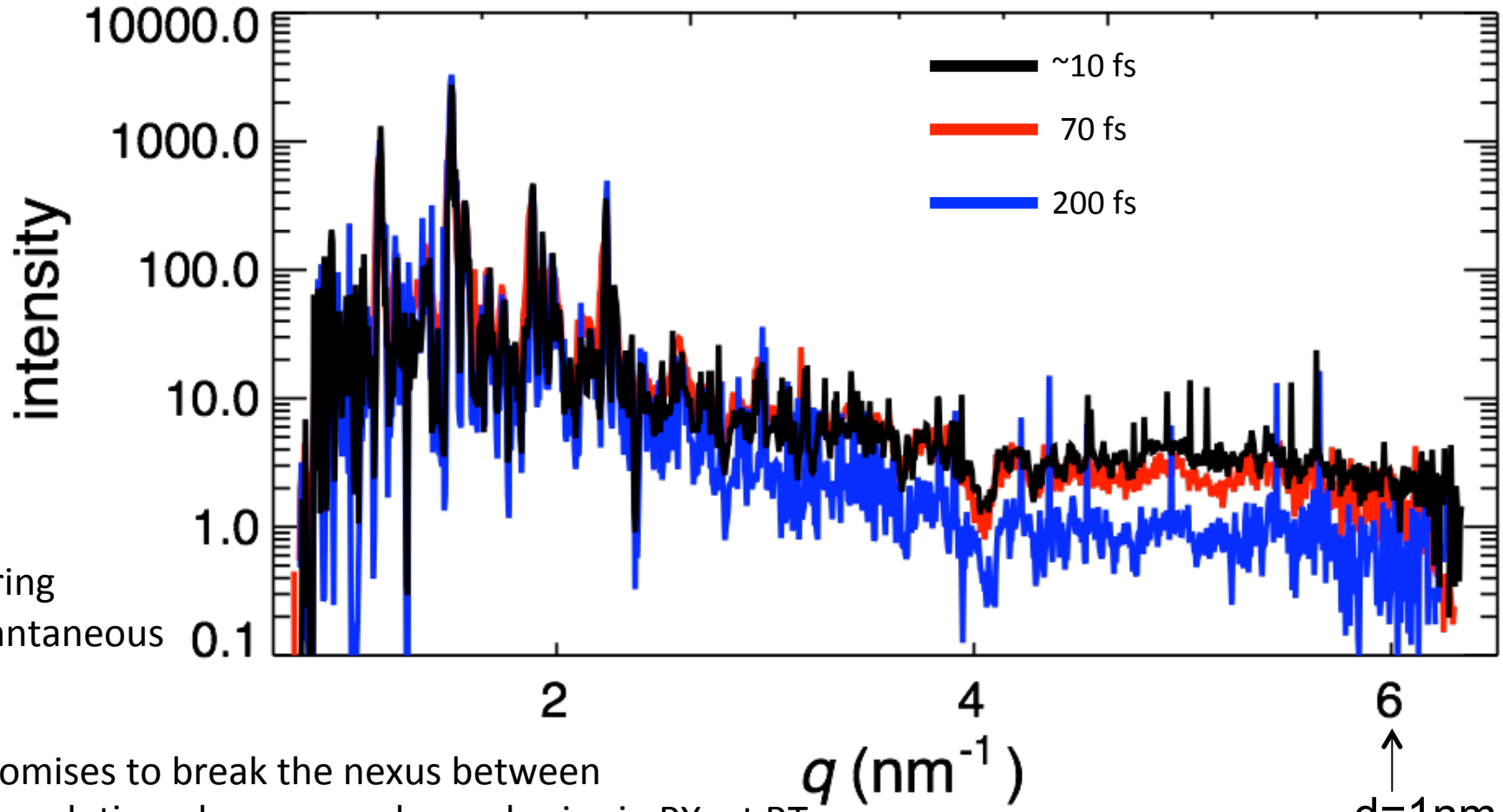

Elastic scattering is instantaneous

SFX promises to break the nexus between dose, resolution, damage, and sample size in PX, at RT

Two modes of particle explosion

Barty et al Nature Photonics 6, 35 (2011).

Future developments

No time for single-virus (Mimi) imaging…..2D published, 3D submitted.
Hajdu, Maia, Eckeberg et al.

Nanoxtal patterns provide new solution to phase problem
Image nucleation and growth ?.

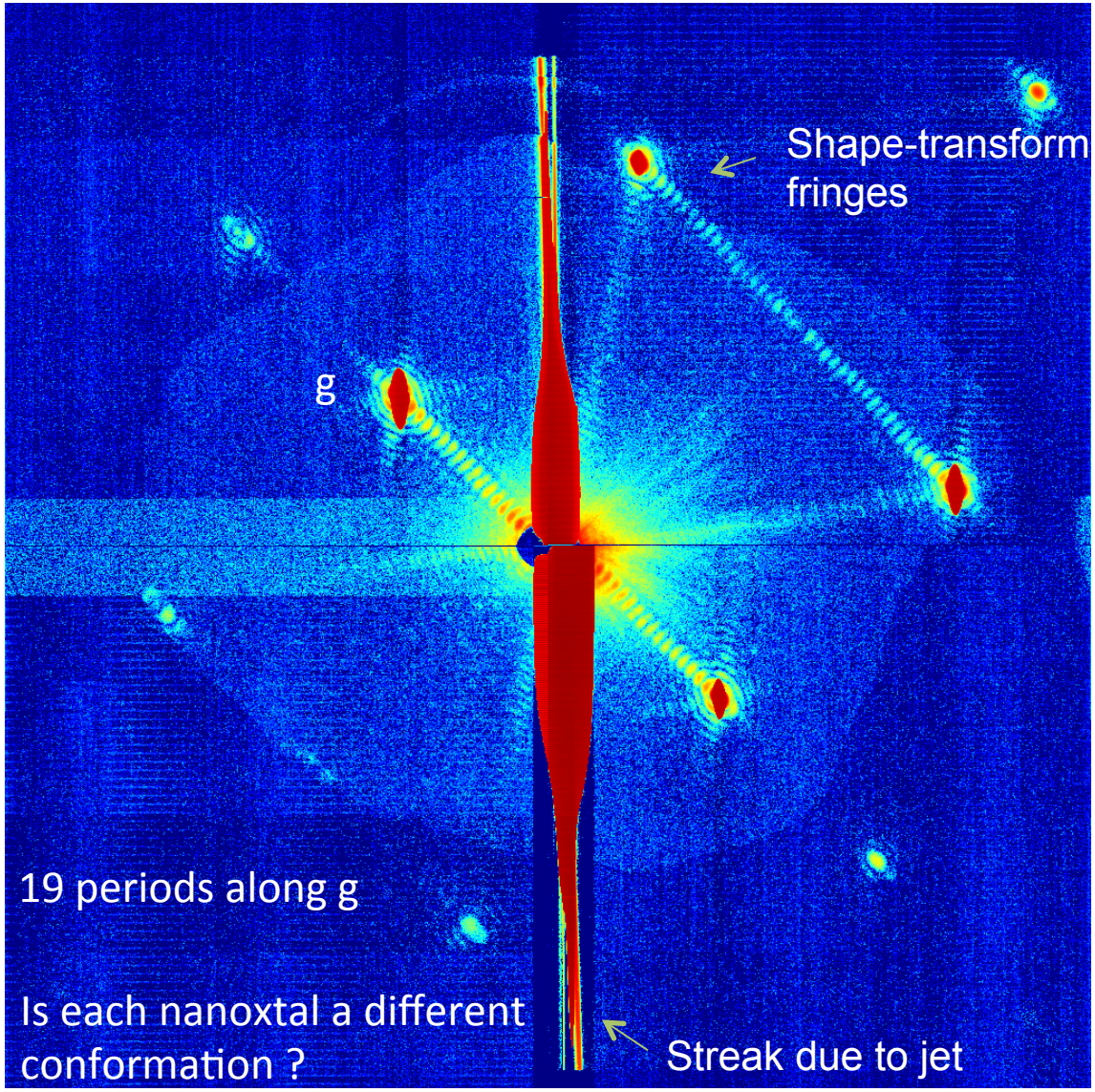

Coherence width spans entire nanoxtal, not cell.

To phase, "divide out" particle size distribution.

Every snap-shot comes from a nanoxtal of different size, with different fine structure on each spot

Every nanoxtal is in a different (random) orientation.

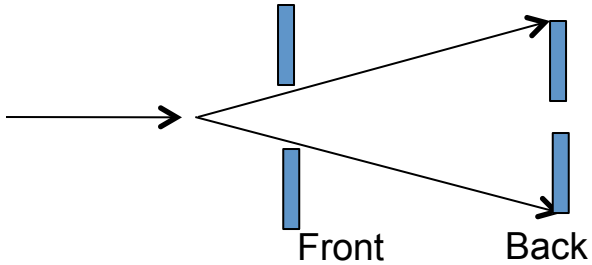

Photosystem I nanocrystals at 2 kV (6.9 Ang wavelength).
Single Shot (10^{12} photons incident).

See Spence et al Optics Express, 2011

Fringes between Bragg spots solves phase problem

F

*We aim to develop a method which uses ALL the data from xtals of different sizes. We are not phasing one nanoxtal.

*The patterns contains information on particle size distribution.

*Each pattern consists of bragg spots broadened by a “shape transform”, with the whole pattern modulated by a “molecular transform”

*Perutz (1949) suggested using gradient of MT across ST.
(vary water content in xtals to change cell dimensions). Sayre 1952.

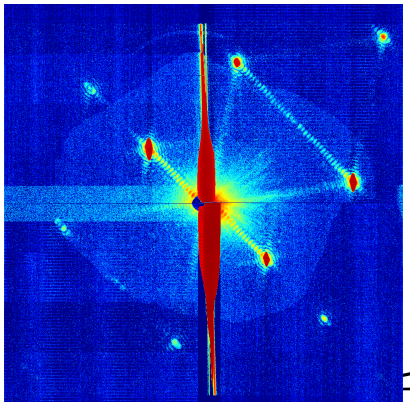

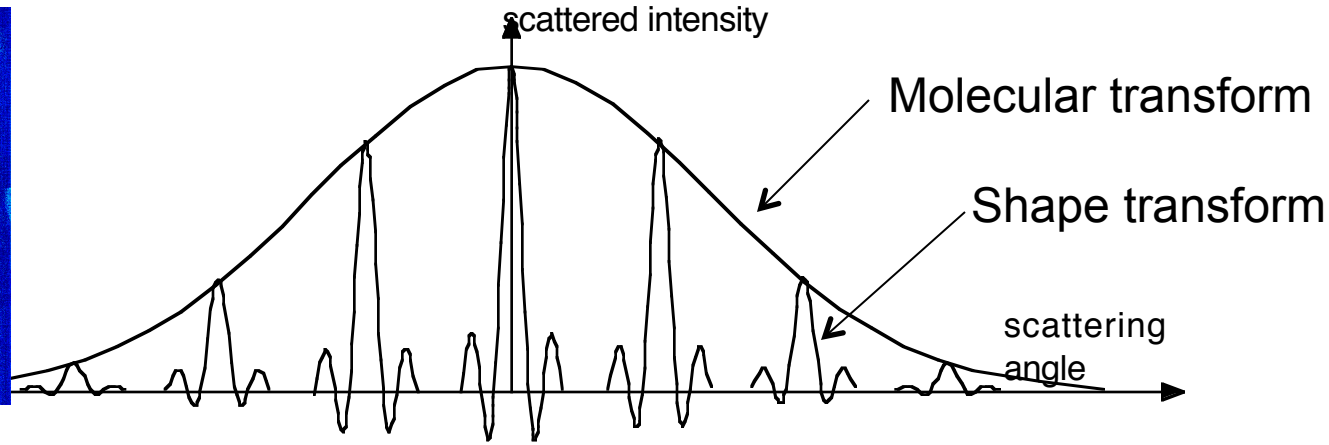

See Spence et al Optics Express, 2011

To use less protein, slow jet speed by using a more viscous medium.
Membrane proteins live in LCP, which is viscous. First results Feb 2012.

"Toothpaste" jet. **GPCR** in LCP at 300 picoliters per minute. LCLS at 1 Hz. 9.4 kV 7%
50 microliters total used Adenosine A2A

Uwe Weierstall

Optimize
conc, rep rate,
viscosity,
particle size,
jet size,
for each
sample.

V = F/A
AV = const.

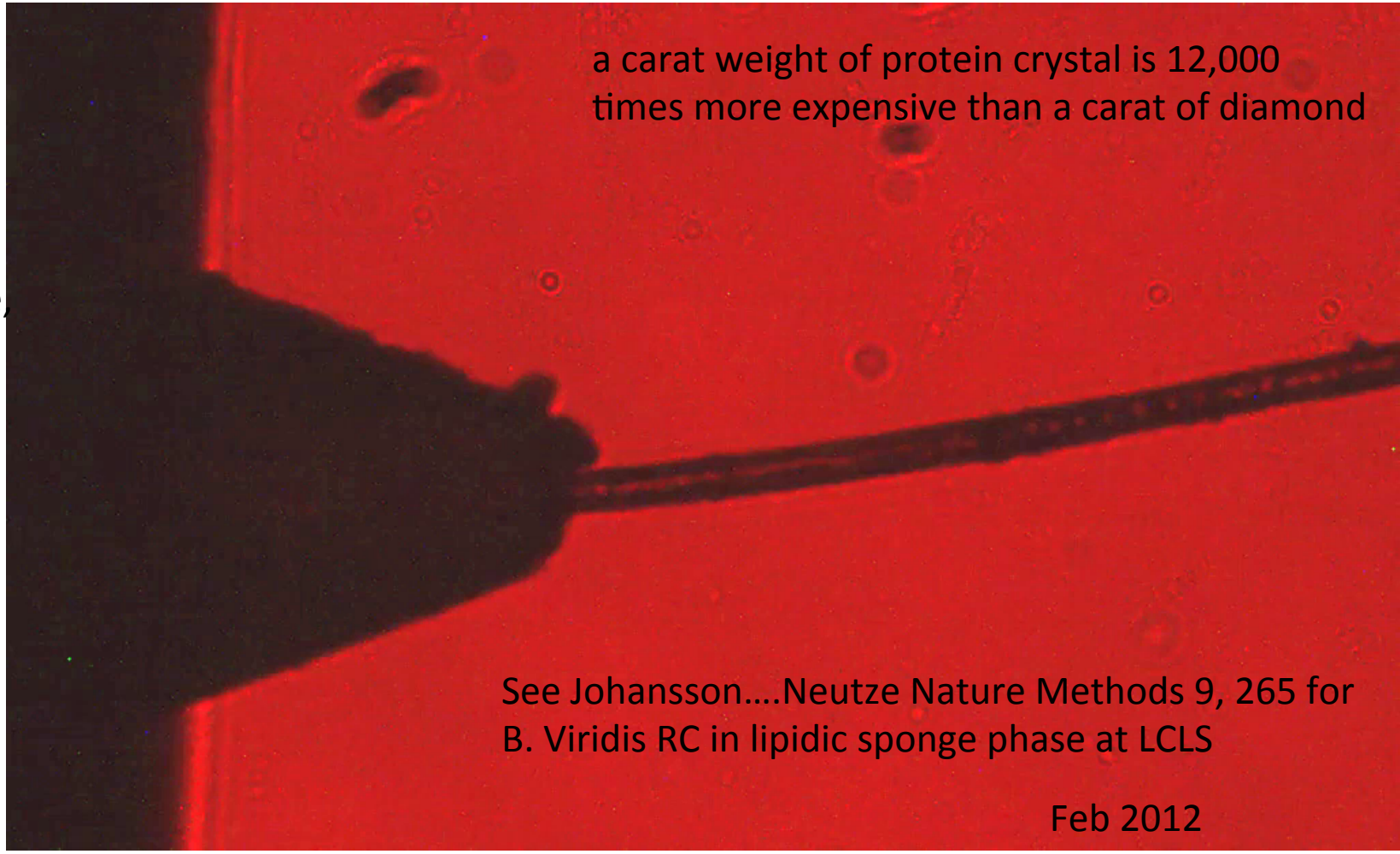

Ray Stevens. High rep rate of NGLS helps

Also Sponge phase , with Richard Neutze.

New hydrated bioparticle injectors being developed at ASU

The dual-bore mixing jet, with gas focusing . Doniac/Pandy. Enzyme chemistry

Wang
Doak
Weierstall
Spence

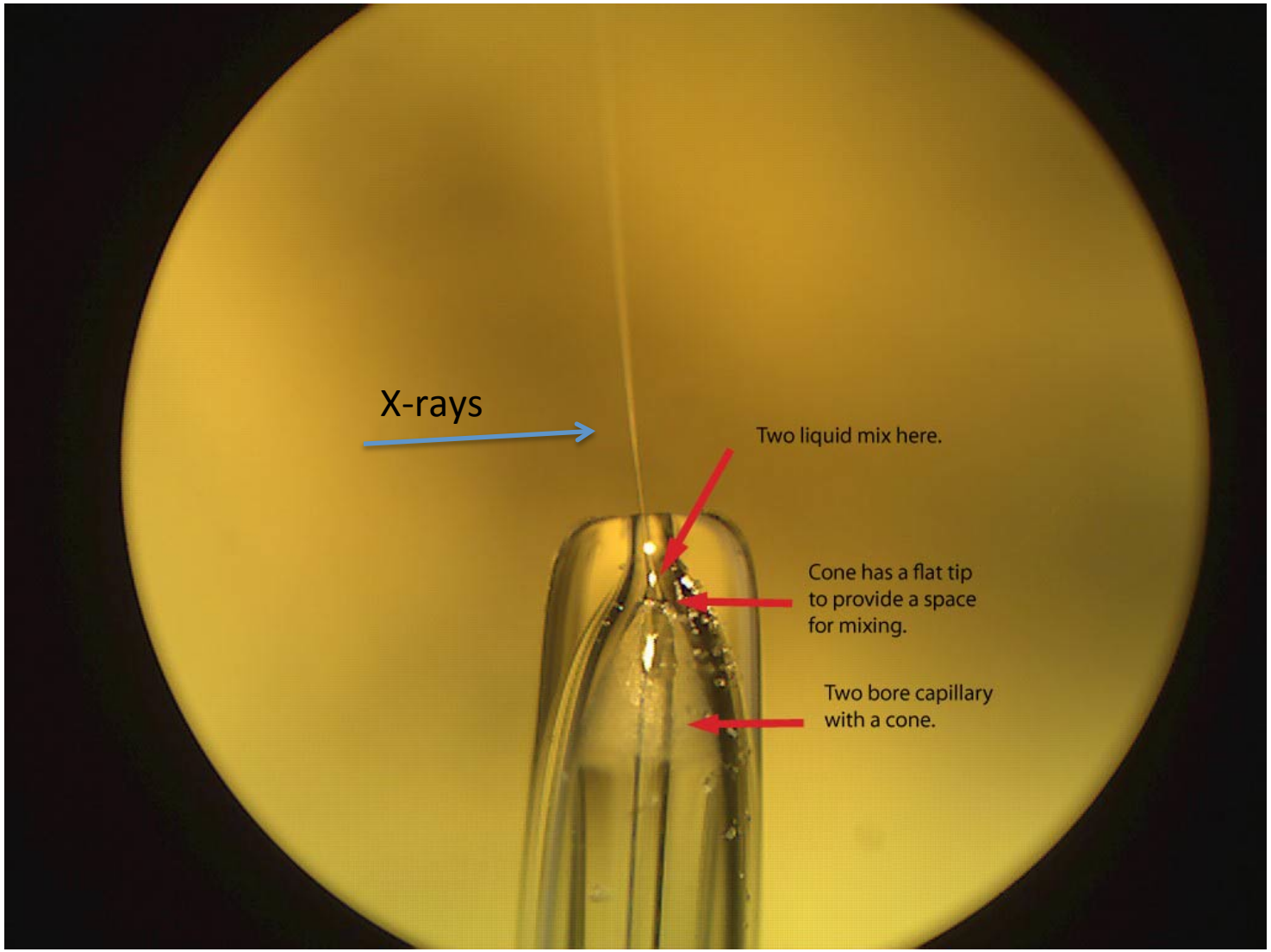

Red Fluor protein RFP. cis-trans due to pH.

"Snapshot chemistry" – watch molecules react.

Dingjie Wang. June 2011

“Snapshot SAXS”

F

* Extracting an image of one particle using the scattering from many copies*

(ab-initio, without SAXS modelling)

* If particles are frozen in space or time, the normally isotropic WAXS pattern becomes 2D

* Hit rate 100% ! No orientation determination !

*identical and randomly oriented. By summing the angular correlation functions we unscramble the orientational disorder.

Fluctuation cross correlations

The experiment consists of detecting scattered intensity at TWO points on a ring, and multiplying these together. Then summing around the ring.

Averaged pair correlations are azimuthally symmetric, they depend only on Δϕ. We measure the angular cross correlation functions in the intensity *fluctuations*:

$$C_2(q,q',\Delta\phi) = \left\langle I'(q,\phi)I'(q',\phi+\Delta\phi)\right\rangle_\phi$$

$$\underbrace{I'(q,\phi) = I(q,\phi) - \left\langle I(q,\phi)\right\rangle_\phi}_{\text{intensity fluctuation (mean subtracted ring intensity)}}$$

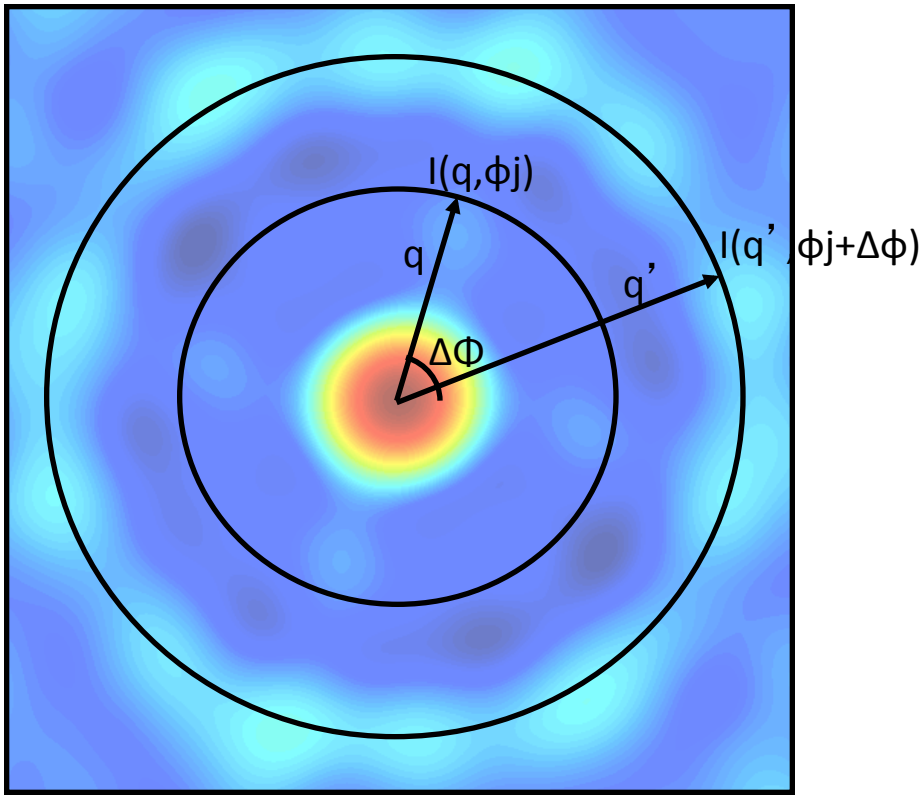

For identical, randomly oriented particles frozen in space or time we can reconstruct an image of one particle, using the scattering from many…

Kam's method unscrambles orientational disorder, ab-initio, without modelling.

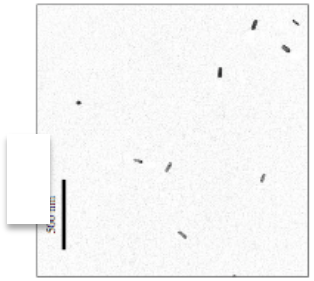

Many identical gold rods.

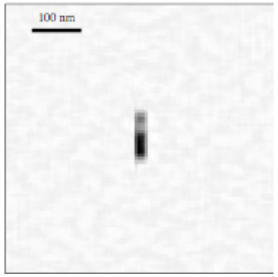

Image of ONE gold rod !!

FT

FT

FT, phasing

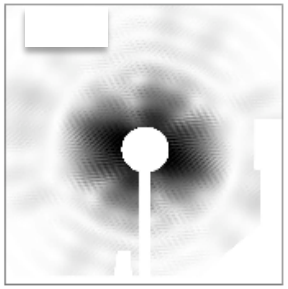

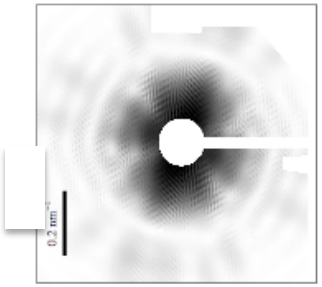

No "SAXS" modelling !

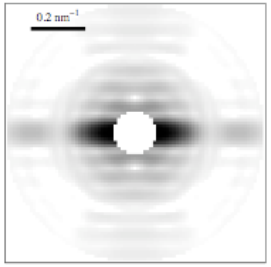

FT, phasing

Angular Autocorrelation Function

+

Angular Autocorrelation Function

+ ……..

=

Angular Autocorrelation Function of ONE partilce

Kam, 1978 ; Saldin, Spence, Kirian PRL 2011, Phys Rev B81, 174175 (2010) Starodub et al 2011.

Experimental demonstration – in two dimensions.

Diffraction patterns were collected from 90nm gold rods
at ALS using coherent 2nm X-rays. Single-axis alignment

TEM Image

Reconstruction from XRD

Now apply this to an enzyme in our mixing jet. Doniach.

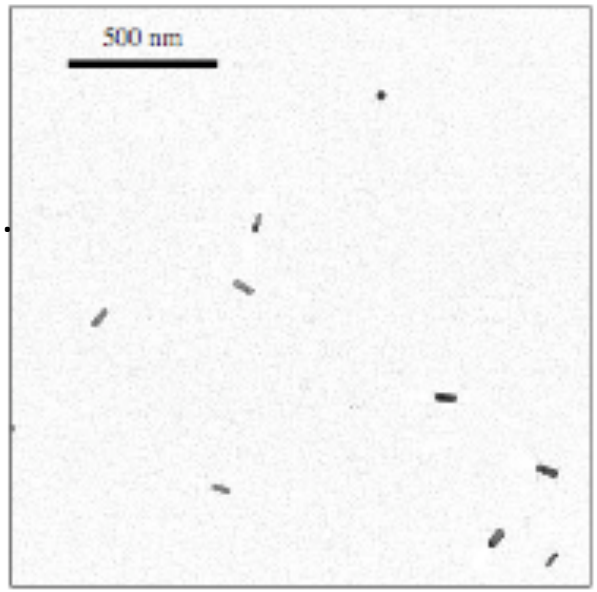

FIG. 1: Electron microscope image of a typical sample from which soft x-ray diffraction patterns are measured. Each sample consists of a set of about 10 gold nanorods of approximately 90 nm × 25 nm projection in random orientations about the normal to a transparent SiN substrate. There is a small admixture of ∼ 25 nm diameter gold nanospheres.

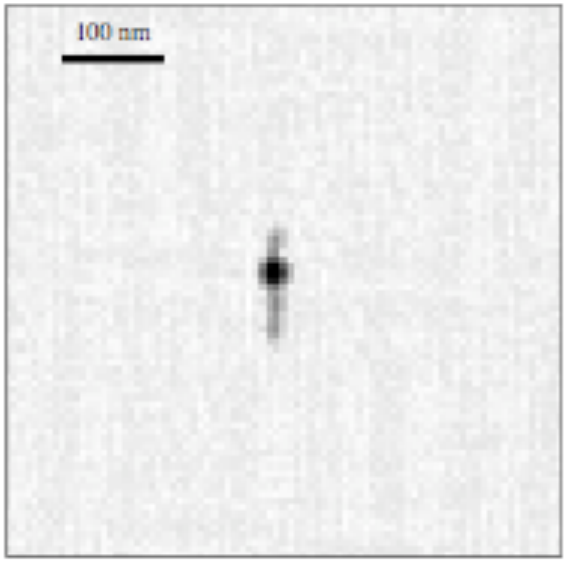

FIG. 7: Projection of the electron density of a single ∼ 90 nm × 25 nm rod reconstructed from the diffraction pattern of Fig. 6 after 100 iterations of the reciprocal-to-real-space phasing algorithm. The bulge near the center is probably a superposition of an image of a nanosphere, also found in the experimental samples (see Fig. 1).

Conformations separated !

In 3D, both beam noise and Kam fluctuations are propn to number of particles, so ratio isn't.
Hence if one particle doesn't work, many won't. Kirian et al submitted. Elser. Wochner.

Saldin, Kirian, Marchesini, Spence…. Phys Rev Letts. 106, 115501 (2011).

Snap-shot SAXS

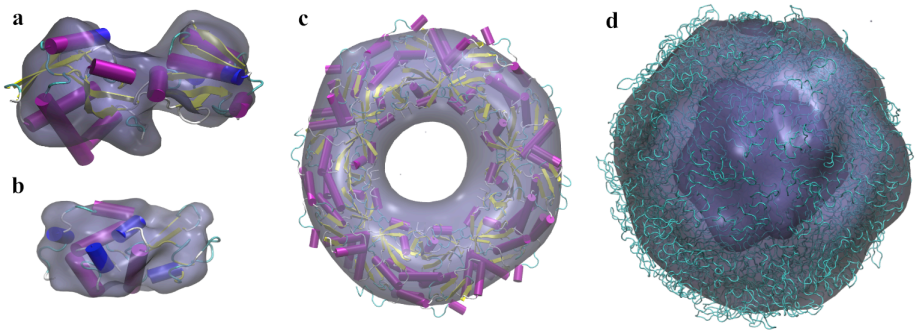

Fig. 3. The four molecular structures used as test cases, superposed on reconstructed density. The models are: a) LAO Binding protein; b) Lysozyme; c) Peroxiredoxin; and d) STMV. Models are not shown to scale. see Table 1 and main text for details

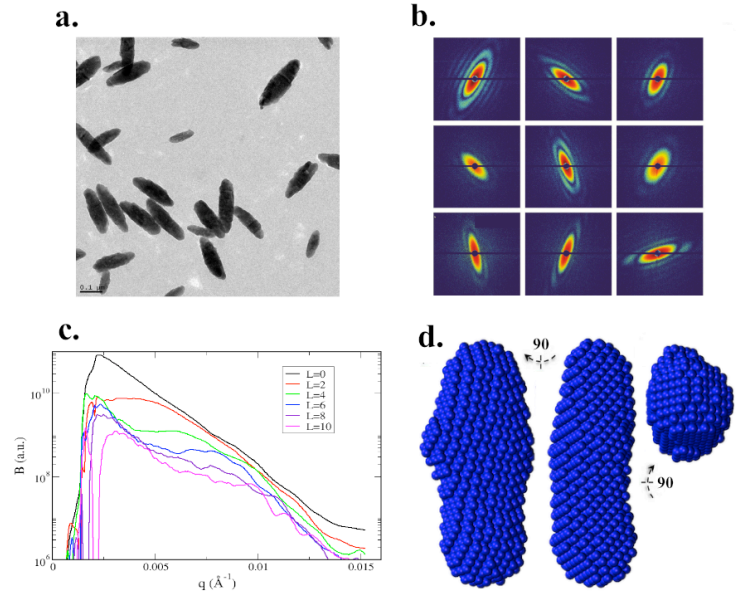

Fig. 4. The reconstruction of the nanorice particle shape from fXS data indicates the feasibility of the method. The TEM images from nanorice (a) show a high similarity to the reconstructed model (d). The diffraction patterns (b) were converted to a fXS data set (c) as described in the main text. a) and b) are reproduced from Kassemeyer *et al.* (2012) with permission from Optical Society of America.

Z. Kam 1978. Snapshot SAXS inversion without modelling, ab-initio. Disentangle..
2D snapshot SAXS from mols frozen in space or time contain more information than conventional 1D isotropic SAXS patterns.

Haiguang Liu, Peter Zwart, John Spence…….submitted. See Poster

An international collaboration

CFEL-DESY

H. Chapman, *J. Schulz, A. Barty, M. Liang, A. Aquila, T. White, D. Deponte, S. Stern, N. Coppola, S. Bajt, M. Barthelmess, A. Martin, C. Caleman, K. Nass, F. Stellato, H. Fleckenstein, L. Gumprecht*

ASU (injector, PS samples, Monte-Carlo method).

J. Spence, *P. Fromme, U. Weierstall, B. Doak, M. Hunter, R. Kirian, K. Schmidt*

SLAC

M. Bogan, *S. Boutet, G. Williams, D. Starodub, R. Sierra, C. Hampton, J. Kryzwinski, C. Bostedt, M. Messerschmidt, J. Bozek*

Uppsala U.

J. Hajdu, *Nic Timneanu, J. Andreasson, M. Seibert, F. Maia, M. Svenda, T. Ekeberg, J. Andreasson, A. Rocker, O. Jonsson, D. Westphal*

LLNL

S. Hau-Riege, M. Frank

LBNL

S. Marchesini, ***J. Holton***

Max Planck CFEL Advanced Study Group

I. Schlichting, *R. Shoeman, L. Lomb, M. Bott, D. Rolles, S. Epp, A. Rudenko, L. Strüder, R. Hartmann, L. Foucar, N. Kimmel,* ***J. Ullrich***

Summary

*Diffractive (lensless) imaging and Ptychography sees inside mesoscopic structure

* Using a TEM, CBED is now a highly quantitative method, used for "seeing bonds".

*X-ray snapshots, without damage, at atomic resolution. Short pulses, instead of freezing allows RT work, hence dynamics, with x100 dose !

*Serial Crystallography solves nanoxtals (eg in bugs, mother liquor). Xtal growth ?

* New "direct" low-res. phasing method, unlimited number of atoms. Fast MAD ?

* Correlated fluctuations in snap-shot SAXS give ab-initio inversion. One from many.

* Fast electron diffraction with new sources may eventually compete with XFEL.

*"On-demand", "Toothpaste" (LCP, Sponge) injectors improve hit rate, less protein

Conclusion: Plenty of diffraction physics remains to be done in static, time-resolved, single particle, fast WAX and nanoxtal "crystallography" .

For a review, see Spence, Weierstall and Chapman, Rep Prog Phys, (2012).

The End

With thanks for many collaborators from CFEL, MPI, ASU,SLAC, Uppsala.

“Biology is a solution in search of a problem; physics a problem in search of a solution”

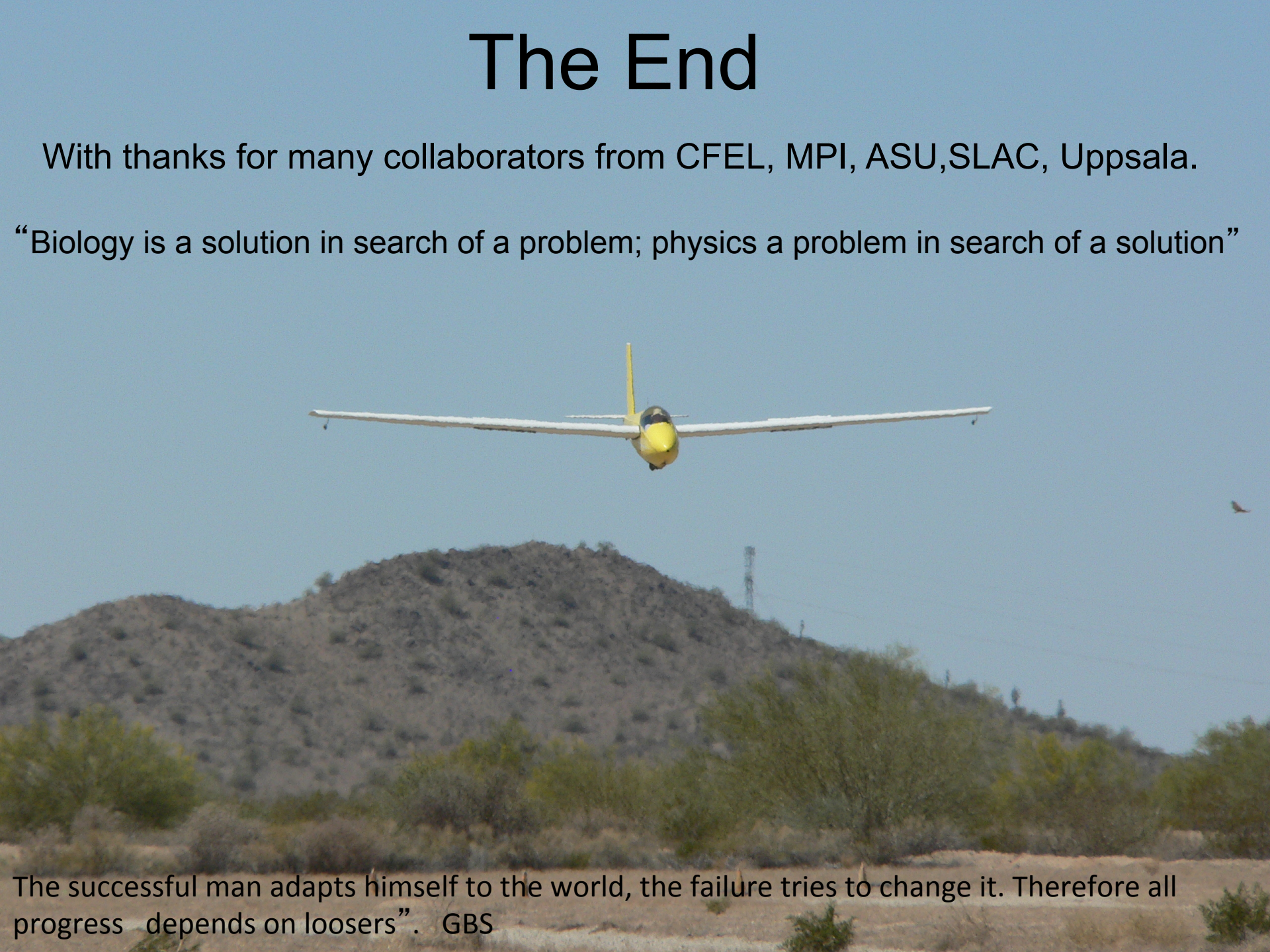

The successful man adapts himself to the world, the failure tries to change it. Therefore all progress depends on loosers”. GBS